TEKNILLINEN KORKEAKOULU
Sähkö- ja tietoliikennetekniikan osasto

Outi Lehmus

MINIATURIZATION METHODS OF HANDSET ANTENNAS

Diplomityö, joka on jätetty opinnäytteenä tarkastettavaksi diplomi-insinöörin tutkintoa varten Espoossa 15.2.1999

Työn valvoja
Professori Pertti Vainikainen

Työn ohjaaja
DI Jani Ollikainen

HELSINKI UNIVERSITY OF TECHNOLOGY

ABSTRACT OF THE MASTER'S THESIS

Author:	Outi Lehmus	
Name of the thesis:	Miniaturization methods of handset antennas	
Date:	February 16, 1999	**Number of pages:** 98
Department:	Department of Electrical and Communications Engineering	
Professorship:	S-26 Radio Engineering	
Supervisor:	Professor Pertti Vainikainen	
Instructor:	Jani Ollikainen, MSc	

In this master's thesis miniaturization techniques of handset antennas were studied. The main requirements set on handset antennas are a broad operating frequency band, high radiation efficiency, and small size. The basic problem in downsizing an antenna is the interrelation between these requirements; an improvement in one property is always at the expense of some other. However, it was discovered that by applying different miniaturization methods, the trade-off contributions could be affected.

At first the general theory of small antennas was studied and a review of the main requirements for mobile handset antennas was given. Then the characteristics of a few potential built-in antenna types appropriate for the use in mobile handsets were presented. These antenna types were dielectric resonator antennas and planar inverted F antennas (microstrip antennas). This was followed by an investigation of different miniaturization methods. The principles of different size reduction techniques were introduced and then the techniques were applied to the studied antenna types.

Several prototype antennas were experimentally investigated. In addition to the normal characterization of impedance and radiation properties, special emphasis was placed on the behavior of radiation efficiency. It was observed that the miniaturization by dielectric loading was efficient with dielectric resonator antennas but it was not a suitable method for the very low-profile patch antenna constructed in this work. When applying high permittivity material into this kind of a structure, the radiation properties deteriorated and the relative contribution of conductor losses grew considerably resulting in a very low efficiency. The miniaturization of planar inverted F antennas by resistive loading was observed to greatly increase the bandwidth, but this occurred directly at the expense of radiation efficiency. Other miniaturization techniques applied to planar inverted F antennas were found to be more or less equal in total performance. The miniaturization by reactive loading was noted to yield high radiation efficiency but the achieved size reduction seemed to waste the bandwidth. The behavior of slow wave structures was similar.

Keywords: Handset antennas, miniaturization, radiation efficiency, bandwidth

TEKNILLINEN KORKEAKOULU **DIPLOMITYÖN TIIVISTELMÄ**

Tekijä: Outi Lehmus

Työn nimi: Käsipuhelinantennien miniatyrisointimenetelmät

Päivämäärä: 16.2.1999 **Sivumäärä:** 98

Osasto: Sähkö- ja tietoliikennetekniikan osasto

Professuuri: S-26 Radiotekniikka

Työn valvoja: Professori Pertti Vainikainen

Työn ohjaaja: DI Jani Ollikainen

Tässä diplomityössä tutkittiin pienten antennien miniatyrisointimenetelmiä. Tärkeimmät käsipuhelinantenneille asetetut vaatimukset ovat laajakaistaisuus, suuri säteilyhyötysuhde sekä pieni koko. Pienentämisen ongelma on näiden vaatimusten keskinäinen suhde; yhden ominaisuuden parantaminen tapahtuu aina jonkin toisen kustannuksella. Työssä havaittiin, että eri miniatyrisointimenetelmiä soveltamalla voidaan vaikuttaa em. ominaisuuksien jakautumiseen.

Aluksi työssä käytiin lyhyesti läpi pienten antennien teoriaa sekä selvitettiin matkapuhelinantenneille asetettuja vaatimuksia. Seuraavaksi esiteltiin muutaman käsipuhelimen sisäiseksi antenniksi soveltuvan antennityypin ominaisuuksia. Käsitellyt antennityypit olivat dielektrinen resonaattoriantenni ja PIFA-antenni (mikroliuskaantenni). Tämän jälkeen tutkittiin eri miniatyrisointitekniikoita ja niiden soveltamista edellä esiteltyihin antennityyppeihin.

Useita antenneja tutkittiin kokeellisesti. Tavallisten impedanssi- ja säteilyominaisuuksien lisäksi mitattiin prototyyppien säteilyhyötysuhteet. Miniatyrisointi dielektrisesti kuormittamalla todettiin tehokkaaksi dielektristen resonaattoriantennien yhteydessä, mutta työssä toteutetulle erittäin ohuelle mikroliuskaantennille, jossa on enemmän metalliosia, tämä menetelmä ei sovi. Korkeapermittiivisen materiaalin lisääminen tällaiseen rakenteeseen heikensi antennin säteilyominaisuuksia aiheuttaen metallihäviöiden suhteellisen osuuden voimakkaan kasvun. Tämä johti hyvin huonoon hyötysuhteeseen. PIFA-antennin resistiivinen kuormittaminen lisäsi huomattavasti kaistanleveyttä, mutta tämä tapahtui selvästi säteilytehokkuuden kustannuksella. Muut PIFA-antenneille sovelletut menetelmät huomattiin kokonaisvaikutuksiltaan melko yhdenvertaisiksi. Reaktiivisesti kuormittamalla saavutettiin korkea säteilyhyötysuhde, mutta antennin koon pienentyessä menetettiin samalla kaistanleveyttä. Sama ilmiö havaittiin hidasaaltorakenteissa.

Avainsanat: Käsipuhelimen antenni, miniatyrisointi, säteilyhyötysuhde, kaistanleveys

Preface

The work for this master's thesis has been carried out in the Radio Laboratory of Helsinki University of Technology (HUT).

I would like to thank my supervisor, Professor Pertti Vainikainen, for the interesting and challenging subject of the thesis as well as all his time he has given to this work. I appreciate his expert advice and numerous valuable suggestions concerning this thesis.

Thanks are due to my instructor Jani Ollikainen for the useful comments to the theoretical part of this work and especially for his skillful assistance in the construction and measurements of the prototype antennas.

I am grateful to all the staff of the Radio Laboratory for their help and support. Especially I would like to thank Lauri Laakso for constructing several prototype antennas.

I would also like to express my warmest thanks to my parents, Airi and Heikki Lehmus, for their support during my entire studies. In addition, thanks are due to my sister Päivi.

Finally, my special thanks are reserved for Kalle for technical assistance and particularly for his love and understanding.

Espoo, February 16, 1999

Outi Lehmus

Table of contents

List of symbols

A	area of capacitive plate
a	resonator width
B_{HP}	half-power bandwidth
B_{max}	maximum obtainable bandwidth
BW	relative bandwidth
b	resonator height
C	capacitance
c	speed of light in vacuum
D	directivity
d	resonator length
d_{CAP}	distance between the capacitive load and the ground plane
d_{CF}	distance between the feed plate and the radiating plate
$\vec{E}$	electric field
f	frequency
f_r	resonant frequency
G	antenna gain
G_r	conductance of antenna
$\vec{H}$	magnetic field
h	antenna height
K	coupling coefficient
k	wave number
k_0	free space wave number
k_x	wave number in x-direction
k_y	wave number in y-direction
k_z	wave number in z-direction
L	inductance
L	length of radiating plate
L_{refl}	reflection loss
L_{retn}	return loss
m, n, p	positive integers referring to the number of electric field maxima
$\vec{n}$	normal vector
P_{in}	input power
P_{in}'	input power including impedance mismatch
P_l	loss power
P_{rad}	radiated power
Q	quality factor
Q_0	unloaded quality factor
Q_c	conductor quality factor
Q_{cd}	quality factor of dielectric and conductor losses
Q_d	dielectric quality factor
Q_e	external quality factor
Q_L	loaded quality factor
Q_r	radiation quality factor
R	distance
R_{cap}	antenna input resistance with the cap

R_{in}	input resistance
R_l	loss resistance
R_r	radiation resistance
R_{uncap}	antenna input resistance without the cap
r	radius
S	maximum VSWR
S_r	power density
S_{11}	scattering parameter
S_{21}	scattering parameter
s	slit length
TE	transverse electric field
TM	transverse magnetic field
t	thickness of the metal conductor
u	dimension
V	volume
$VSWR$	voltage standing wave ratio
W	width of radiating plate
W	stored energy
W_e	stored electric energy
w	width of short circuit
w_s	width of slit
x	distance between the short circuit and the position of the feed probe
Y_0	characteristic admittance of transmission line
Y_{LC}	parallel admittance
Z	impedance

$\tan\delta$	loss tangent
ε_0	permittivity in vacuum
ε_r'	real part of relative permittivity
ε_r''	imaginary part of relative permittivity
η_r	radiation efficiency
λ_0	free space wavelength
λ_r	wavelength in the dielectric media
μ_0	permeability in vacuum
ρ	reflection coefficient
ρ_{min}	minimum reflection coefficient
ρ_r	reflection coefficient at resonant frequency
σ_c	conductivity
ω	angular frequency
ω_r	angular resonant frequency

List of abbreviations

DRA	dielectric resonator antenna
DWM	dielectric waveguide model
HUT	Helsinki University of Technology
HV-DRA	half-volume dielectric resonator antenna
MSA	microstrip antenna
MWM	magnetic wall model
PEC	perfect electric conductor
PIFA	planar inverted F antenna
SAR	specific absorption rate
UMTS	Universal Mobile Telecommunication System
WCM	Wheeler cap method

1 Introduction

Currently the trend is to miniaturize the components in all parts of electronics because of the advances in integrated circuits. This progress has lead to a significantly decreased size of a mobile telephone unit. The size and the shape of a handset have a great importance regarding the convenience and portability. The handset size, however, is limited by the size of the battery and the size of the antenna. As the handset size becomes even smaller, there is insufficient space for a conventional antenna. More stringent requirements on antenna dimensions provoke attempts to overcome the size problem.

In these respects the tendency of handset antennas is in miniature built-in ones, in which the entire antenna is installed inside the handset casing on a small ground plane. With such merits as mechanical durability and directivity characteristics, built-in antennas could replace conventional external "stick-out" antennas in some applications. The placement of the antenna on the back side of the handset casing results in a radiation pattern that points away from the user's head regardless of the antenna type. This reduces the potentially harmful effects of microwave radiation on human tissue and improves antenna efficiency; less power is absorbed into the user.

On the other hand, demands set on the electrical properties of handset antennas are increasing all the time. The new personal communications systems, e.g. UMTS, are likely to offer multimedia services that call for broader operating frequency band than the current systems. Additionally, modern handsets need to operate in various systems and thus in several frequency bands. The output power of a mobile handset will be

reduced and the radiation efficiency of a handset antenna has to be increased due to the limited power available. The necessity of broadband and efficient antennas complicates the antenna miniaturization. The main difficulty in downsizing an antenna is the interrelation between antenna volume, bandwidth, and radiation efficiency; an improvement in one property is always at the expense of some other.

There are already certain built-in handset antennas in the market, but working miniature antenna solutions are still insufficient even though the physical problems with reducing the antenna size are known. This thesis aims at collecting information on different miniaturization techniques of built-in handset antennas and studying the basic rules for miniaturization. The purpose is to establish guidelines and to find the general laws for predicting the behavior of miniaturized antennas.

This thesis is organized into seven chapters. Chapter 2 gives a review of the general theory of small antennas. Definitions for essential antenna terms are presented. Also limitations on miniaturization and requirements for handset antennas are discussed. The studied antenna types, including dielectric resonator antennas and planar inverted F antennas, are briefly introduced in Chapter 3. Chapter 4 presents different miniaturization techniques and summarizes their characteristics. The miniaturization methods are applied to antenna types presented in Chapter 3. In Chapter 5 some applications with prototype antennas are introduced and measurement results are reported. The results are discussed in Chapter 6. The work is concluded in Chapter 7.

2 Small antennas

In this chapter the general theory of small antennas is presented. That includes definitions for the essential terms, discussion about limitations on antenna size reduction and a review into requirements for handset antennas.

2.1 FUNDAMENTALS

Near its fundamental resonance any small antenna can be approximated as a resonant circuit, where a feed arrangement is added, since small antennas are always resonators. A resonator can be defined as a structure that has a natural frequency of oscillation [1]. A resonant antenna is purely resistive at the resonant frequency and no conjugate matching circuit between the antenna and the load is needed. The resonance can be achieved either by the antenna element itself or by using active, passive, or material loading.

The nature of small antennas is problematic. Antenna size, bandwidth, and efficiency are interrelated and there is not complete freedom to independently optimize each one. The matching of a small antenna can be achieved efficiently only over a narrow bandwidth [2]. The smaller the antenna size relative to the wavelength is, the narrower the achievable bandwidth becomes. When reducing the antenna size, the radiated power also decreases in comparison to the ohmic losses. This decreases the antenna efficiency. Hence, designing small antennas is always a trade-off between antenna size, bandwidth, and efficiency.

2.1.1 Definition of a small antenna

A small antenna can be defined in terms of size, wavelength, and function. Generally speaking, the size of a small antenna is a small fraction of the operating wavelength. Its greatest dimension is typically limited to be smaller than ¼ λ_0, including any image due to ground plane [3]. Here, λ_0 is the free-space wavelength.

More theoretical definitions for a small antenna can be divided into four categories: electrically, functionally and physically small, and physically constrained antennas [4].

An electrically small antenna can be enclosed by a radiansphere, which is a hypothetical sphere of radius equal to one radianlength $\lambda_0/2\pi$ [5]. The radiansphere is the nominal boundary between the reactive near field and the far field.

A physically constrained antenna has a significant size reduction in one plane. Nevertheless, it does not inevitably satisfy the definition of an electrically small antenna. Planar antennas belong to this antenna class because their heights are very low electrically.

A functionally small antenna has additional functions without antenna size increase. For example, an asymmetrically driven dipole antenna can have beam-shifting function, which would usually require an array of dipole elements [4]. Either functionally small antennas are not necessarily electrically small.

A physically small antenna has a relatively small size even though it does not have to belong into any category above. Millimeter-wave horn antenna is an example of a physically small antenna.

2.1.2 Bandwidth

Broadly speaking, an antenna bandwidth is a frequency range which can be limited by different parameters like gain, beamwidth, side-lobe, or reflection level. In general the useful bandwidth of an antenna depends on both its impedance and pattern characteristics where polarization characteristics are included [6]. When dealing with small antennas, the term bandwidth typically refers to the impedance bandwidth. In literature the most commonly used definition for the impedance bandwidth of small antennas is the frequency range in which the return loss $L_{retn} \geq 10$ dB (or $VSWR \leq 2$, which is almost equal). At the moment $L_{retn} \geq 6$ dB for the whole operating frequency range has also been accepted by mobile antenna industry [7]. In this thesis the definition $L_{retn} \geq 6$ dB is followed.

Comparable to return loss, equal parameters can be expressed for the absolute value of the reflection coefficient $|\rho|$ and for the voltage standing wave ratio *VSWR*. Also power loss due to the mismatch between the antenna and the feed can be stated. This reflection loss L_{refl} can be given in decibels or in percent of the total input power. Corresponding values for $|\rho|$, *VSWR*, and L_{refl} to L_{retn} = 10 dB and L_{retn} = 6 dB are listed in Table 2.1. The values are calculated according to the following equations:

$$L_{retn} = 10\log_{10}\frac{1}{|\rho|^2} \tag{2.1}$$

$$VSWR = \frac{1+|\rho|}{1-|\rho|} \tag{2.2}$$

$$L_{refl} = 10\log_{10}\frac{1}{1-|\rho|^2}. \tag{2.3}$$

Table 2.1 *Corresponding values for $|\rho|$, VSWR, and L_{refl} when L_{retn} = 10 dB and L_{retn} = 6 dB.*

L_{retn} [dB]	$\|\rho\|$	VSWR	L_{refl} [dB]	L_{refl} [%]
6.00	0.50	3.01	1.26	25
10.0	0.32	1.92	0.46	10

2.1.3 Quality factors

The quality factor Q of a resonator, like that of a resonant antenna, can be defined as its ability to store electromagnetic energy. Accordingly, Q is the ratio of the stored energy to the radiated or lost energy per period:

$$Q = 2\pi f_r \frac{W}{P_l}, \tag{2.4}$$

where f_r is resonant frequency, W is stored energy, and P_l is loss power.

An equivalent circuit for a resonant antenna is presented in Figure 2.1. The transmission line describing the antenna feed is loaded with a parallel resonant circuit, i.e. the actual antenna element.

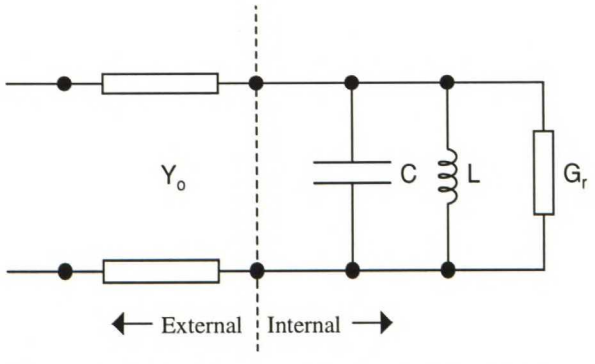

Figure 2.1 *Equivalent circuit of a resonant antenna.*

When a resonant circuit is used as a load in a microwave circuit, several different quality factors can be defined. Unloaded quality factor Q_0 accounts for internal losses of the resonator. The resonator is connected to an external circuit (antenna feed). Part of the stored energy escapes through this external connection. Similarly, external quality

factor Q_e accounts for external losses. The quality factors can be defined with the parameters in the equivalent circuit in Figure 2.1 [8]:

$$Q_0 = \frac{\omega_r C}{G_r} = \frac{1}{\omega_r L G_r} \tag{2.5a}$$

$$Q_e = \frac{\omega_r C}{Y_0} = \frac{1}{\omega_r L Y_0}. \tag{2.5b}$$

Here, ω_r is angular resonant frequency, C is the capacitance, G_r is the conductance, and L is the inductance of the antenna, and Y_0 is the characteristic admittance of the transmission line feeding the antenna.

The parameters in the equivalent circuit can also be stated as a function of the quality factors, i.e. there is no need to know the circuit parameters. When the characteristic admittance of the transmission line is normalized to unity ($Y_0 = 1$) and the resonance condition $\omega_r = 1/\sqrt{LC}$ is applied, the parallel admittance of the reactive components can be written as $Y_{LC} = jQ_e(\omega/\omega_r - \omega_r/\omega)$, where ω is angular frequency. Correspondingly the conductance can be written as a ratio of the quality factors $G_r = Q_e/Q_0$. This is the inverse of the definition of the coupling coefficient K, which will be presented later in this section.

If $Q_e > Q_0$, the internal losses dominate over the external and the resonator is undercoupled. Correspondingly, if $Q_0 > Q_e$, the resonator is overcoupled. If $Q_e = Q_0$, the coupling is critical and the resonator is matched to the feed at the resonant frequency.

Loaded quality factor Q_L is the overall quality factor including both internal and external losses:

$$\frac{1}{Q_L} = \frac{1}{Q_0} + \frac{1}{Q_e}. \tag{2.6}$$

The unloaded quality factor of a resonator with one connection (i.e. antenna feed) can be linked to the loaded quality factor also as follows [1]:

$$Q_0 = \frac{2Q_L}{1 \pm |\rho_r|}, \tag{2.7}$$

where ρ_r is the reflection coefficient at the resonant frequency. The plus sign is used in the undercoupled and the minus sign in the overcoupled cases. If the antenna is perfectly matched, Equations (2.6) and (2.7) simplify to $Q_0 = 2\ Q_L$.

Equation (2.7) is useful considering measurements, as Q_0 can not be measured directly but it can be calculated from the easily measured Q_L. The unloaded quality factor is an important figure-of-merit of a small resonant antenna. It is due to all the losses in the cavity or resonator itself. The loss power can be divided into radiation, conductor, and dielectric losses:

$$\frac{1}{Q_0} = \frac{1}{Q_r} + \frac{1}{Q_c} + \frac{1}{Q_d}, \tag{2.8}$$

where Q_r is radiation quality factor, Q_c is the quality factor of conductor losses, and Q_d is dielectric quality factor. For an efficient antenna operation Q_r should be dominant.

According to [1], the quality factor Q_c due to the loss in the metal parts is proportional to the square root of the frequency:

$$Q_c \propto \frac{\omega \int_V |\vec{H}|^2 dV}{\sqrt{\omega} \int_S |\vec{H}|^2 dS} \sim \sqrt{\omega}\ . \tag{2.9}$$

Here, ω is angular frequency, $\int_V |\vec{H}|^2 dV$ is the volume integral and $\int_S |\vec{H}|^2 dS$ is the surface integral of the square of the magnetic field in the resonator.

In reality the fields of a resonant antenna are partly in air and partly in the dielectric. If the fields are approximated to be entirely inside the resonator, the calculation of dielectric quality factor Q_d can be made according to [9]

$$Q_d = \frac{1}{\tan\delta}, \tag{2.10}$$

in which $\tan\delta$ is the loss tangent of the dielectric material used to fill the volume of the resonator. The loss tangent is defined as

$$\tan\delta = \frac{\varepsilon_r''}{\varepsilon_r'}. \tag{2.11}$$

Here, ε_r' is the real part and ε_r'' is the imaginary part of the relative permittivity.

On the other hand, Q-factor is a merit of how selective the resonance is. Unloaded quality factor Q_0 is inversely proportional to the relative bandwidth BW of the antenna. Hence, the greater antenna losses (including radiation) are, the smaller Q_0 is and the wider BW becomes. For a $VSWR$ of less than S, the relative bandwidth of a resonant type antenna can be given as [10]

$$BW = \frac{1}{Q_0}\sqrt{(KS-1)(1-\frac{K}{S})}, \tag{2.12}$$

Here, K is a coupling coefficient indicating the quality of matching:

$$K = \frac{Y_0}{G_r} = \frac{Q_0}{Q_e}. \tag{2.13}$$

When the coupling coefficient K = 1, the antenna is matched to the transmission line and the relative bandwidth can be written as follows:

$$BW = \frac{S-1}{Q_0\sqrt{S}}. \tag{2.14}$$

Nevertheless, the perfectly matched antenna does not give a theoretical maximum bandwidth. Instead, the maximum bandwidth can be achieved when the antenna is slightly overcoupled and the coupling coefficient satisfies the equation [10]

$$K = \frac{S^2+1}{2S}. \tag{2.15}$$

Thus the maximum value for the bandwidth can be expressed as

$$BW_{\max} = \frac{1}{Q_0}\frac{S^2-1}{2S}. \tag{2.16}$$

2.1.4 Radiation efficiency

Radiation efficiency η_r is the ratio of the radiated power and the total loss power of the antenna:

$$\eta_r = \frac{Q_0}{Q_r} = \frac{Q_r^{-1}}{Q_r^{-1}+Q_c^{-1}+Q_d^{-1}}. \tag{2.17}$$

For a lossless antenna $Q_r = Q_0$.

By combining Equations (2.14) and (2.17), the relation between relative bandwidth and radiation efficiency can be illustrated for a matched antenna. As can be seen from Equation (2.17), the radiation efficiency of a small antenna decreases when increasing conductor and dielectric losses. The effect of increased internal losses on relative bandwidth is presented in Figure 2.2, where the radiation efficiency is described as a function of relative bandwidth. Radiation quality factor Q_r is chosen to be 11.6, which

corresponds to the relative (6 dB) bandwidth of 10 % when the original antenna is assumed to be lossless.

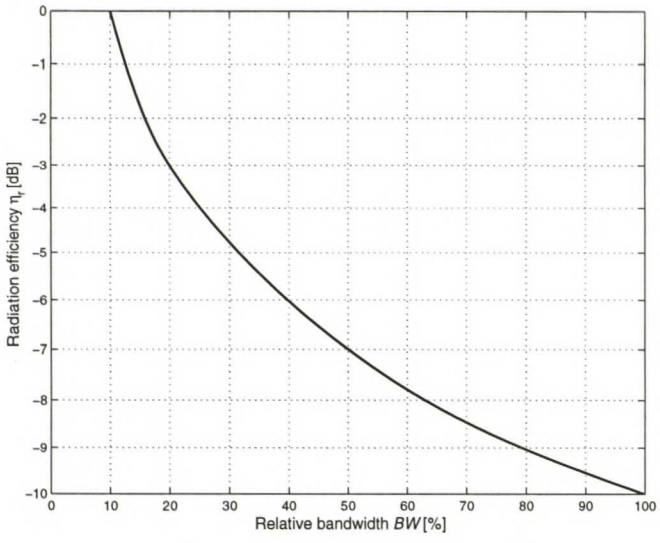

Figure 2.2 *Radiation efficiency of a small antenna as a function of relative bandwidth.*

As shown in Figure 2.2, the radiation efficiency is reduced by 3 dB, i.e. to half of the original value, when doubling the relative bandwidth by increasing internal losses. Correspondingly, when the relative bandwidth is four times the original, the efficiency falls to fourth of the original value.

2.1.5 Gain and directivity

Absolute gain of an antenna is defined as the ratio of the power density in a given direction to the power density that would be obtained if the antenna input power was radiated isotropically [11]:

$$G = 4\pi R^2 \frac{S_r}{P_{in}}. \tag{2.18}$$

Here, S_r is power density, P_{in} is antenna input power, and R is the distance from the antenna. The gain is taken in the direction of maximum radiation when the direction is not otherwise stated.

Although P_{in} is the power at the antenna input port, it is not the actual power accepted by the antenna since there occurs reflection losses due to antenna mismatch to the feed. The gain definition does not include losses arising from impedance mismatches. However, when considering small antennas these are significant losses and they need to be taken into account. For the bandwidth criterion of $L_{retn} \geq 6$ dB, the reflection loss due to mismatch can be $L_{refl} = 1.26$ dB at the edge of the operating frequency band, as stated in Table 2.1. This would mean a significant gain uncertainty if the feed mismatch was excluded. Therefore $P_{in}' = P_{in}(1-|\rho|^2)$ could be used as a preferable definition for the power at antenna input port. Here, ρ is the reflection coefficient at the antenna feed.

In many cases a relative gain is used. It can be defined as the ratio of the power gain in a given direction to the power gain of a reference antenna in its referenced direction. In most cases, the reference antenna is a lossless isotropic source. The same considerations regarding impedance mismatches are valid here.

Gain can be related to the directivity D by radiation efficiency:

$$G = \eta_r D . \tag{2.19}$$

The directivity of an antenna is defined as the ratio of the power density in a given direction from the antenna to the radiated power density averaged over all directions [11]:

$$D = 4\pi R^2 \frac{S_r}{P_{rad}}, \tag{2.20}$$

where P_{rad} is the radiated power from the antenna. The impedance mismatches should also be considered here.

2.2 LIMITATIONS ON SIZE REDUCTION

Antenna dimensions can not be diminished endlessly without antenna performance being affected. The free-space wavelength has a settled value depending simply on the operating frequency. The antenna element must couple to this free-space wave [12].

The fundamental limit, as to how small an electrically small antenna element can be made, is derived by assuming the entire antenna structure enclosed within a sphere of radius r. Equivalent sources distributed on the surface of the sphere are considered to form the antenna radiation [13]. Outside the sphere the radiated field can be presented by orthogonal spherical wave modes [14]. Each mode represents an outward radial direction propagating spherical wave. There is no coupling between any modes outside the sphere [11]. All wave modes contribute to the reactive power of the antenna while only the propagating modes form the radiated power [12].

Q_0 is calculated in terms of the nonpropagating energy external to the sphere and the radiated power [14]. Higher order modes become evanescent (below cutoff) for roughly $kr < 1$ [12]. The system quality factor for the lowest order TE or TM mode becomes [14]:

$$Q_0 = \frac{1}{k^3 r^3} + \frac{1}{kr}, \tag{2.21}$$

where k is wave number and r is the radius of the smallest sphere enclosing the antenna.

Equation (2.21) gives the minimum theoretical unloaded quality factor that can be achieved assuming a lossless antenna (except for radiation losses). The quality factor is independent of the geometrical configuration of the antenna within the sphere of radius r. However, the antenna shape determines which wave modes are excited [11].

According to Equation (2.21), for $kr << 1$, Q_0 varies inversely as the cube of sphere radius in radian wavelengths. As the antenna element size decreases, Q_0 grows rapidly. When the sphere containing the antenna element becomes very small no propagating

modes exist; all modes are below cutoff and carry only little power, storing a great amount of energy inside the sphere. Q_0 turns into a very large value [12].

When both TE and TM mode are excited, the minimum possible Q_0 can be expressed as [14]:

$$Q_0 = \frac{1}{2}\left(\frac{1}{k^3 r^3} + \frac{2}{kr}\right). \tag{2.22}$$

The combined TE and TM fields produce circularly polarized fields. Since TE and TM modes are dual, they have the same Q_0 value. Nevertheless, the minimum Q_0 of a circularly polarized antenna, presented in Equation (2.22), is only approximately half that of a linearly polarized antenna (Equation (2.21)). This is because the TE mode stores predominantly magnetic energy in its nonradiating fields but also some electric energy and vice versa [14].

When there are several propagating modes, Q_0 is calculated from the contributions of all the individual modes [15]. Equations for the quality factor for each of the spherical modes individually are derived in [13].

In Equations (2.21) and (2.22) a lossless antenna is assumed. The losses can be included by applying Equation (2.17) together with Equations (2.21) and (2.22). The minimum achievable unloaded quality factor for an idealized single mode antenna as a function of kr is shown for various efficiencies in Figure 2.3. The results are obtained utilizing Equations (2.17) and (2.21).

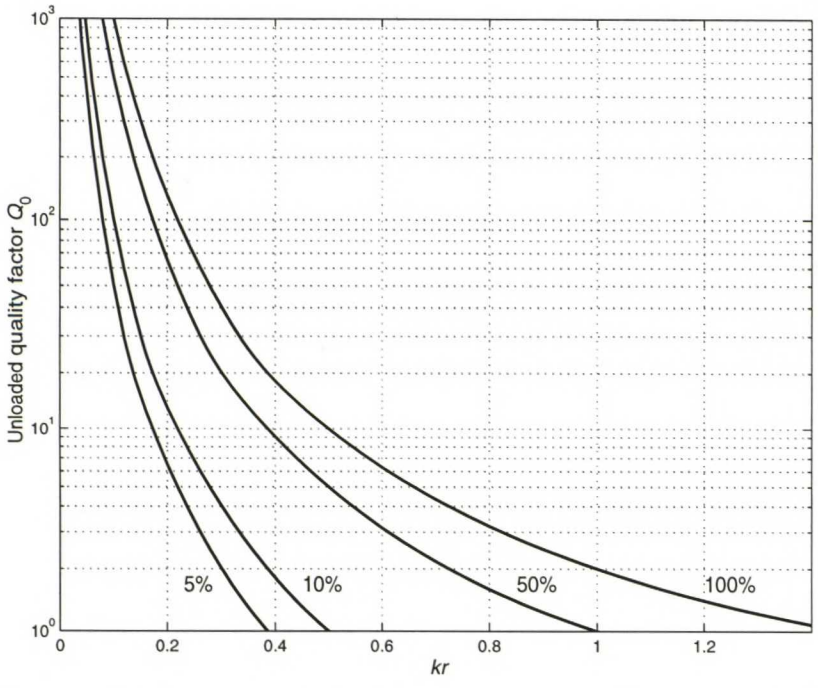

Figure 2.3 *Minimum achievable unloaded quality factor Q_0 for a linearly polarized antenna as a function of kr for various efficiencies (η_r = 100%, 50%, 10%, 5%).*

Fundamental limit on the electrical size of the antenna can be approached but never reached or exceeded. An antenna exciting only the lowest order mode, either TE or TM, and storing no energy inside the sphere, has the lowest possible radiation Q_0 of any linearly polarized antenna [14]. Getting the system quality factor near the theoretical minimum limit is possible by entirely utilizing the volume limited by a sphere of radius *r*. In practice, antennas do not completely make use of the spherical volume. In addition, also other wave modes are excited than just the lowest ones [14]. In reality these additional modes as well as the lowest order modes always store energy also within the sphere; this inevitably increases the value of Q_0.

On the whole, any attempt to reduce the physical size of an antenna while preserving the same resonant frequency ends up with deficiencies such as bandwidth reduction and reduction in efficiency. Efforts on performance evaluations are often experimental; it is difficult to predict the exact antenna performance theoretically.

2.3 REQUIREMENTS FOR HANDSET ANTENNAS

Handset antennas must satisfy stringent requirements concerning geometrical characteristics, electrical performance which must not be degraded by the nearby user context, manufacturing costs, and safety standards concerned with potential health risks. The rapid development of personal communications systems leads continuously to new, stricter demands.

Wire antennas have been the dominant type of radiators in portable handsets until now. In order to meet all the requirements of new communications systems, traditional monopole and helical antennas are not longer adequate, even though they have many great advantages. Replacing external antennas with internal is a future trend, at least built-in antennas are potential alternatives to the traditional ones.

2.3.1 Physical characteristics

In a mobile handset there is only a limited space provided for an antenna on the surface of the equipment. Thus, antennas are required to be small in volume and light in weight. A convenient shape of a mobile casing calls for compact and low-profile antenna structures. The aim is at built-in types; in addition to stable and handy mechanical structure they would also reduce the overall size of the phone.

2.3.2 Electrical characteristics

Since the handset operates close to the human body, the effect of electromagnetic energy must be taken into account. The specific absorption rate (SAR) towards user produced by a traditional monopole should be reduced, even though there is no scientific proof on harmful effects of microwave radiation of a handset antenna. The placement of the antenna on the back side of the mobile casing reduces the fields in the vicinity of the user's head since the handset works as a reflector between the antenna and the head.

Because the conducting casing acts as a ground plane, the antenna currents flow also on the casing. Hence the whole portable unit has to be included in antenna system as a part of radiator when analyzing an antenna [16]. The current distribution will be disturbed when a hand grips around the handset, which implies that both the antenna impedance and radiation pattern will change. Accordingly, the effect of user on antenna performance has to be as small as possible; an antenna must fulfill requirements in free space as well as beside the human body.

An omnidirectional radiation pattern reduces the radiation efficiency since a lot of radiated power is lost into the head and hand of the user. Hence, uniform radiation over azimuthal angle in a hemisphere away from the user would be a desirable feature. That can be implied by mounting the antenna on the back side of the mobile casing; a resulting radiation pattern points away from the user's head regardless of the antenna type.

The polarization of a handset antenna depends upon the position of the phone. For a fixed receiver (a base station) the polarization seems arbitrary due to the random orientation of the phone and to several propagation paths (reflection, diffraction, scattering) in the environment. For that reason, the polarization of a handset antenna is not likely to be significant in urban environment whereas in rural area or line-of-sight-environment it is more important. Resulting from this, specifying the required polarization of the phone is not easy. Traditionally vertically polarized handset antennas have been used.

A handset antenna should have an adequate bandwidth covering the frequency range used by the system. The detailed requirements of operating frequency and bandwidth are different for each system. Typically, the impedance bandwidth requirement could be defined as the return loss of $L_{retn} \geq 6.0$ dB for the whole operating frequency range. This means that it is accepted in the specifications that up to 25 % of the total input power is lost due to the mismatch.

The transmitting power of a portable handset must be kept low because of limited battery capacity. The radiation efficiency should be as high as possible due to the restricted power available. The value of η_r should preferably be better than 90 %.

A handset antenna should also provide sufficiently high gain over the operating bandwidth. The gain of a small antenna is typically low and is even degraded due to the proximity of the human body. The minimum sufficient gain is about 0 dBi for an omnidirectional radiator [16]. For a directive internal antenna this value should be higher. Typical directivity of an internal handset antenna is 3... 5 dBi. For the radiation efficiency value of $\eta_r \approx 90$ % this gives the gain requirement of about 2.5... 4.5 dBi using gain definition of Equation (2.19). When considering also the impedance mismatch, as discussed in Section 2.1.5, the gain requirement becomes correspondingly different.

2.3.3 Fabrication considerations

From the fabrication point of view, a handset antenna should have a simple structure and suitability for mass production. All the components must include a safety margin for production tolerances. The mounting of the antenna on portable equipment should not be complex.

People are probably unwilling to buy more expensive handsets because of increased antenna cost. Therefore new built-in antenna types ought to have competitive price with traditional handset antennas.

3 Studied antenna types

In this chapter a few different antenna types appropriate for the use in mobile handsets are introduced. The antenna configurations chosen are dielectric resonator antennas and planar inverted F antennas. These antenna types are selected because of their potential as built-in handset antennas and the diversity of miniaturization methods suitable for portable applications with these antenna categories. The most important characteristics of the chosen antenna types are studied. These characteristics include antenna size, resonant frequency, radiation, bandwidth, loss mechanisms, and feeding methods.

3.1 DIELECTRIC RESONATOR ANTENNAS

3.1.1 Introduction

A dielectric resonator antenna (DRA) is an antenna which simply consists of a block of relatively high permittivity material ($\varepsilon_r' \approx 6...100$) situated on top of a conducting ground plane [17]. Image theory can be applied when the ground plane is assumed infinite and the ground plane can be replaced by an imaged portion of the dielectric structure. A dielectric resonator antenna offers several advantages. It can have various shapes but it still keeps up mechanical simplicity, flexible design and feeding methods, low cost, and light weight. There is no excitation of surface waves in DRAs and dielectric losses are very small [18]. Excluding feed, a conventional DRA does not comprise metal portions. Hence its operation is not limited by intrinsic conductor loss. Though, all practical DRAs reported so far employ a metallic plane [19], and there exist

conductor losses induced in the metallic plane on which the resonator is placed. Thus the harmful loss of a dielectric resonator antenna is mainly caused by conductor loss in the ground plane. These losses are typically small, and this antenna type has a high radiation efficiency.

This work concentrates only on rectangular dielectric structures because of their feasibility for handset applications and easiness of fabrication compared to other shapes. Rectangular resonators have also one more dimensional parameter than cylindrical resonators: two aspect ratios *b/a* (*height/width*) and *d/a* (*length/width*) can be chosen independently. Furthermore, in rectangular structures the mode degeneracy and hence a high cross-polarization level can be avoided by properly choosing the dimensions of the resonator [20]. However, rectangular DRAs have been less frequently used in practice so far. Structure of a rectangular dielectric resonator antenna is presented in Figure 3.1.

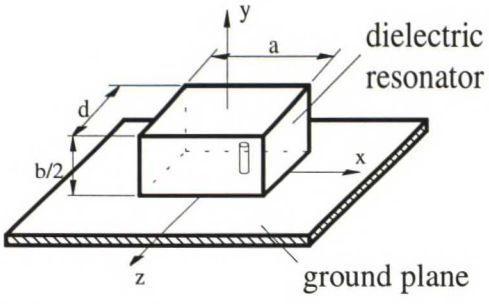

Figure 3.1 *Structure of a rectangular dielectric resonator antenna.*

3.1.2 Size

The dimensions of a DRA are approximately proportional to $(\varepsilon_r')^{-1/2}$ because the wavelength in the resonator material, λ_r, depends on the value of the relative permittivity ε_r' of the material:

$$\lambda_r = \frac{\lambda_0}{\sqrt{\varepsilon_r'}}. \tag{3.1}$$

Hence the volume of a DRA increases by a factor of eight each time the frequency is halved or the relative permittivity value is reduced to fourth. Consequently, a compact-size antenna is most easily achievable with a high relative permittivity material and for a high frequency region.

Since the size of the resonator decreases with an increase in the relative permittivity ε_r', a very high material permittivity value can offer a tiny DRA. However, it is claimed that dielectric resonator antennas with a relative permittivity value greater than $\varepsilon_r' \approx 20$ are not very suitable for antenna applications because of their poor bandwidth characteristics [21].

Dielectric resonator antennas are used above a ground plane; this way the physical size of the cavity height can be halved. If the width and the length of a rectangular antenna on top of a conducting ground plane are much greater than the height ($a, d >> b/2$), the height can be calculated by an approximate equation [21]

$$b/2 \approx \frac{\lambda_0}{4\sqrt{\varepsilon_r'}}. \tag{3.2}$$

The other two cavity dimensions have to be chosen according to the resonant frequency and the wavemode to be excited. The resonator dimensions, desired mode, and the resonant frequency are closely related to each other as will be reported in Section 3.1.3. It is important to notice that antenna shape and aspect ratios affect the antenna performance significantly.

3.1.3 Modes, resonant frequency and radiation

The modes of a rectangular DRA have not been well understood and for the present there is no rigorous technique for evaluating them [22]. Still, there are two common approximate methods for analyzing rectangular resonators: the magnetic wall model (MWM) method [23] and the dielectric waveguide model (DWM) method [24]. In magnetic wall model an approximate solution for the fields inside the cavity can be

obtained by assuming the resonator surfaces being perfect magnetic conductors. Then equivalent magnetic surface currents can be calculated. Those equivalent currents are considered to be the sources for the far-field radiation. According to the dielectric waveguide model, it can be assumed that the resonator is a truncated section of an infinite dielectric waveguide and the standing wave patterns in x- and y-directions inside the resonator are governed by the characteristic equations of the isolated infinite waveguide [24]. By combining the two models presented above, a computationally simple mixed model used below is obtained. In that, the resonator surfaces $|z| = d/2$ are assumed to be imperfect magnetic conductors while the remaining four surfaces are assumed to be perfect magnetic walls.

Using the MWM, the wave numbers k_x and k_y for a *mnp*-mode can be written as

$$k_x = \frac{m\pi}{a},\ k_y = \frac{n\pi}{b}, \tag{3.3}$$

where a is the width and b is the height of the isolated resonator, m and n are positive integers, which refer to the number of electric field maxima in the standing wave pattern along the x- and y-directions.

Since the magnetic wall boundary condition $\vec{E} \cdot \vec{n} = 0$ does not hold at the $|z| = d/2$ surfaces, the DWM is here utilized. A transcendental equation for the wave number k_z can be obtained [24]:

$$k_z \tan(\frac{k_z d}{2}) = \sqrt{(\varepsilon_r' - 1)k_0^2 - k_z^2}\ . \tag{3.4}$$

Here, d is the length of the resonator and k_0 is the free-space wave number at the resonant frequency. It can be defined as follows

$$k_0 = \frac{2\pi}{\lambda_0} = \frac{2\pi f_r}{c}, \tag{3.5}$$

in which c is the velocity of light in vacuum and f_r is resonant frequency.

The wave numbers k_x, k_y and k_z also satisfy the separation equation

$$k_x^2 + k_y^2 + k_z^2 = \varepsilon_r' k_0^2 . \tag{3.6}$$

The resonant frequency defines at which frequency the oscillating fields create the strongest energy inside the structure. As can be seen from the above expressions, the dimensions of the cavity and the material permittivity value determine the resonant frequencies of different modes. When the aspect ratios *b/a* and *d/a* decrease, the resonant frequency increases, provided that the width a is kept constant [18].

Location of the feed and the used excitation method determine which wave modes are actually excited. The equivalent currents for the excited mode on assumed perfect magnetic walls are used to compute the fields in the region outside the resonator. To compute the fields inside the resonator, the same equations are used, but with the sign of the computed currents changed and with all medium parameters set to those of the dielectric resonator. Magnetic wall boundary condition $\vec{E} \cdot \vec{n} = 0$ holds at the surfaces $|x| = a/2$ and $|y| = b/2$ of the resonator. Therefore the electric field inside the resonator is tangential to these surfaces. Only when the excitation is at the resonant frequency of a mode, radiation takes place efficiently and the field is usually dominated by a single mode. If several wave modes are excited, several resonant frequencies can exist. Different modes of the resonator can be utilized to obtain different radiation characteristics.

When the dimensions of DRA are such that $a > b > d$, the lowest order mode excited in rectangular dielectric resonator antennas is $TE^z_{11\delta}$-mode. The field components for that mode can be written as [20]:

$$H_z = \frac{k_x^2 + k_y^2}{j\omega_r \mu_0} B \cos(k_x x) \cos(k_y y) \cos(k_z z) \tag{3.7a}$$

$$H_x = \frac{k_x k_z}{j\omega_r \mu_0} B \sin(k_x x)\cos(k_y y)\sin(k_z z) \tag{3.7b}$$

$$H_y = \frac{k_y k_z}{j\omega_r \mu_0} B \cos(k_x x)\sin(k_y y)\sin(k_z z) \tag{3.7c}$$

$$E_x = Bk_y \cos(k_x x)\sin(k_y y)\cos(k_z z) \tag{3.7d}$$

$$E_y = -Bk_x \sin(k_x x)\cos(k_y y)\cos(k_z z) \tag{3.7e}$$

$$E_z = 0 \tag{3.7f}$$

Here, B is an arbitrary constant, ω_r is angular resonant frequency, and μ_0 is the permeability in vacuum.

The fields of the $TE^z_{11\delta}$-mode are presented in Figure 3.2. It is worth noting that the figure presents an isolated resonator. The radiation pattern of rectangular DRA, excited with $TE^z_{11\delta}$-mode, is similar to that of a horizontal z-directed magnetic dipole placed on a conducting plane.

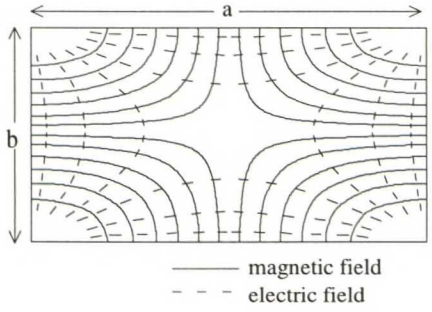

Figure 3.2 *Electric and magnetic fields of* $TE^z_{11\delta}$ *-mode inside an isolated rectangular dielectric resonator, side view.*

3.1.4 Loss mechanisms and quality factors

In DRAs, the dominant loss mechanism is radiation. The radiation quality factor can be determined using the relation

$$Q_r = \frac{2\omega_r W_e}{P_{rad}}, \tag{3.8}$$

where ω_r is angular resonant frequency, W_e is stored electric field energy, and P_{rad} is radiated power. The electric field energy equals the magnetic field energy and hence the total stored energy W [see Equation (2.4)] can be stated as $2W_e$. For a rectangular DRA radiating the lowest order mode, W_e can be given by the following equation [20]:

$$W_e = \frac{\varepsilon_0 \varepsilon_r' abdB^2}{32}(1+\frac{\sin k_z d}{k_z d})(k_x^2 + k_y^2). \tag{3.9}$$

The radiated power can now be written as [20]

$$P_{rad} = 10k_0^4 \left| -\frac{j8B\omega_r \varepsilon_0(\varepsilon_r' - 1)}{k_x k_y k_z} \sin(\frac{k_z d}{2})\vec{u}_z \right|^2. \tag{3.10}$$

In the above equations k_x, k_y, k_z, and k_0 are determined from Equations (3.3)-(3.6) , and B is an arbitrary constant.

According to [20], it then follows that

$$Q_r \propto (\varepsilon_r')^{3/2}. \tag{3.11}$$

When comparing the above equation to Equation (3.1) it is found that the radiation quality factor is inversely proportional to the antenna volume: $Q_r \propto V^{-1}$.

According to [22], Equation (3.11) is valid for all modes that radiate like a magnetic dipole but only for antennas of very high permittivity. Nevertheless, it is found in the same reference that Q_r values follow to a decent approximation the relation of Equation (3.11) even for moderate values of ε_r', even though the value of the exponent term may slightly differ.

It also follows from Equations (3.8)-(3.10) that

$$Q_r \propto (1/f_r)^3. \tag{3.12}$$

From Equation (3.12) it can be seen that $Q_r \propto V$. Therefore, when the resonator dimensions are scaled only according to resonant frequency and the material permittivity value is kept constant, the radiation quality factor stays constant [18].

From Equation (3.11) it can be noticed that the DRA size reduction by dielectric loading increases the radiation quality factor. On the other hand, this at the same time increases the resonant frequency value which in turn decreases the radiation quality factor [see Equation (3.12)]. This interrelation between the relative permittivity value and the resonant frequency makes the miniaturization complicated.

In addition to the radiated power, some power is lost in the dielectric material and in the metallic parts. Dielectric losses of DRAs are typically very small although they normally increase when the permittivity value increases. The dielectric quality factor Q_d is inversely proportional to losses and independent of the dimensions of the antenna as stated in Equation (2.10).

In basic DRA structures there are no inherent conductor losses. But conductor losses induced in the metallic plane under the DRA may have an effect on the radiation efficiency. An expression for the quality factor of conductor losses was given in Equation (2.9). It shows that Q_c is proportional to the square root of the frequency and to a dimension u of the antenna. According to Equation (3.1), DRA dimensions are inversely proportional to the square root of the relative permittivity ε_r' of the material. Combining these two conditions, the Q_c of a DRA with certain shape can be written in the following form

$$Q_c \sim \sqrt{\omega} \cdot u \propto \sqrt{\omega} \cdot \frac{1}{\sqrt{\varepsilon_r'}}. \tag{3.13}$$

3.1.5 Bandwidth

The bandwidth of a DRA can be varied over a wide range, from a few percent up to ten percent or more. Typically, with a single dielectric element only smaller bandwidth values can be reached, and a relatively wide bandwidth calls for multiple elements or bulky individual elements. The bandwidth is inversely proportional to unloaded quality factor, as discussed in Section 2.1.3. Thus the bandwidth as well as the size of the resonator increases with a decrease in the relative permittivity value. The bandwidth can also be increased by choosing a lower value for the aspect ratio *d/a* of the resonator [18]. The bandwidth can be controlled as well by adjusting the shape, aspect ratio and the relative permittivity value of the antenna.

3.1.6 Overview of feeding methods

Antenna input impedance can be defined as voltage-to-current ratio at the antenna input terminals [1]. Input impedance can be controlled by choosing a right excitation method and the impedance matching can be achieved by adjusting the feed location as well as dimensions. Several excitation methods for dielectric resonator antennas have been investigated such as the coaxial probe [25], microstrip fed aperture [18], microstrip line [26], and coplanar waveguide [27]. Feeding by a coaxial probe and aperture coupling seem to be the most common ones, coplanar waveguide excitation is seldom used.

Probe excitation means that a dielectric structure is excited by a monopole probe (for example, an extended inner conductor of a coaxial cable) inserted from beneath the ground plane into the dielectric (see Figure 3.3). In order to have the strongest coupling to the antenna, the probe is placed into the electric field maximum inside the resonator. The outer conductor of the coaxial line is connected to the ground plane. At higher frequencies this kind of excitation induces significant metallic loss as well as large probe self-reactances. Nevertheless, it is very suitable for experiments because it is easy to manufacture.

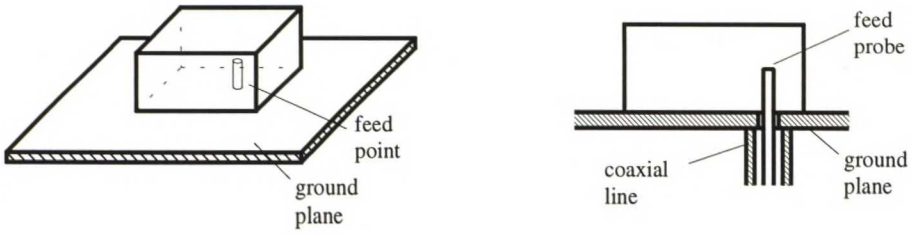

Figure 3.3 *Coaxial feed mechanism for a rectangular DRA.*

In aperture coupling a dielectric resonator is placed above a slot etched in the ground plane of a microstrip line which runs on the other side of the dielectric substrate (see Figure 3.4). The aperture couples the energy from the microstrip line to the dielectric resonator. To excite a lowest order mode of a rectangular-shaped DRA, the antenna has to be kept symmetrical with respect to the slot. The aperture must not resonate within the operating frequency band, otherwise it increases radiation to the back of the antenna and hence reduces the radiation efficiency on the front side. Aperture coupling method increases the total thickness of the antenna structure. Though, one remarkable benefit is the low interference between the DRA and the feed network because no physical connection between them is needed.

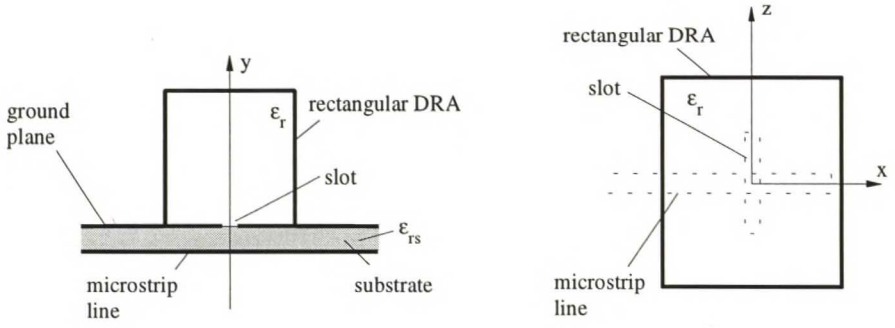

Figure 3.4 *Excitation of a rectangular DRA by aperture-coupling a) side view b) top view.*

In microstrip line excitation the DRA is put on the microstrip side of the ground plane. A microstrip line can be strongly coupled to the DRA but on the other hand, the DRA is on the same side as the feed network and thus it is not isolated from active circuitry; this may cause spurious radiation and coupling.

3.2 PLANAR INVERTED F-ANTENNAS

3.2.1 Introduction

A planar inverted F antenna (PIFA) can be considered as an air-filled, short-circuited microstrip antenna (MSA) that allows a simple impedance match in a low-profile design. On the other hand a PIFA can be thought of as a linear inverted F antenna where the wire radiator element has been replaced by a plate to expand the bandwidth. A PIFA typically consists of a rectangular radiating plate, a ground plane, a short circuit between them and a feed probe. The radiating element is parallel to the ground plane, and is short-circuited at one corner. The short circuit is normally implemented by a vertical plate element or a shorting pin. The distance between the plate and the ground plane is short in wavelengths, typically $0.02\lambda_0 \ldots 0.08\lambda_0$. A basic PIFA structure is illustrated in Figure 3.5.

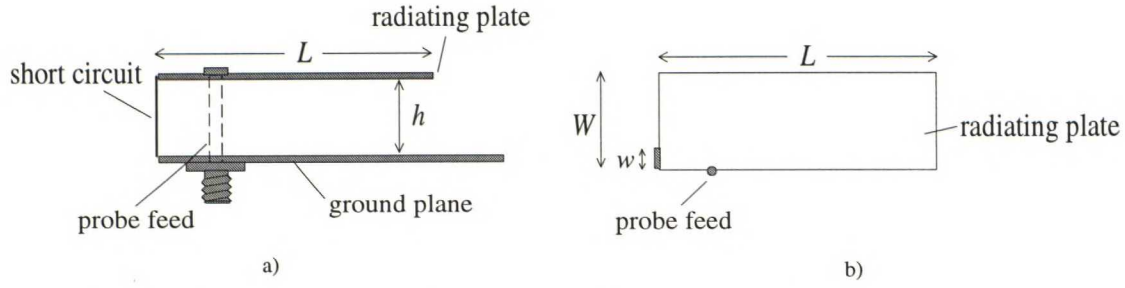

Figure 3.5 *Configuration of a planar inverted F antenna a) side view b) top view.*

PIFA design variables are the antenna height, the top plate dimensions, the location of the feed as well as the width and location of the short circuit. Many different variables make antenna design to be quite a difficult task but it also creates numerous possibilities.

PIFA is one of the most promising candidates to be used as an internal handset antenna and, in fact, it has already been used in handsets. PIFA has many attractive features. It is quite simple and inexpensive to manufacture. It can be made compact with a low profile. No additional matching networks are needed because the matching can be achieved by varying the feed location. PIFA has a relatively wide bandwidth. It can (depending on the configuration) receive both vertically and horizontally polarized

waves, which is important with portable radio equipment where antenna orientation is not fixed.

3.2.2 Size

Planar inverted F antenna is a $\lambda/4$-resonator even though typical resonant antennas are $\lambda/2$-structures. The short circuit at one edge of the radiating element of the PIFA allows the antenna size to be reduced by a factor of two for a given resonant frequency; the shorted edge halves the size of the resonant structure from $\lambda/2$ to $\lambda/4$.

The resonance condition depends on the width and on the location of the short circuit plate. When placing the short circuit plate into the edge of the radiating element the resonant frequency is lower compared to the case when the short circuit is in the middle of the plate. The length of the PIFA is reduced by fabricating the short circuit plane narrower than the radiating plate; the effective inductance increases and the resonant frequency becomes lower [28]. The two uttermost cases are when the short circuit is equal to the total length of the radiating plate and when it is only a wire at the corner of the radiating element. The resonance condition in these two particular cases can be written [28] :

$$L + h = \lambda / 4 \; for \; w / W = 1 \tag{3.14}$$

$$W + L + h = \lambda / 4 \; for \; w = 0. \tag{3.15}$$

Here, W is the width and L is the length of the radiating plate, w is the width of the short circuit and h is the height of the antenna, i.e. the distance between the ground plane and the radiating plate (see Figure 3.5).

3.2.3 Resonant frequency and radiation

Mostly the length of the top plate controls the resonant frequency [29] but the location of the short circuit has influence on that, too, as discussed in the previous section. The resonant frequency varies also with the size ratio *W/L* of the radiating plate and the width *w* of the short circuit plate since the current flow varies, as shown in Figure 3.6. When the short circuit plate has a full width, the surface currents flow straightforward away from the short circuit. While the short circuit is narrower, the effective length of the surface current paths is increased causing a decrease in the resonant frequency.

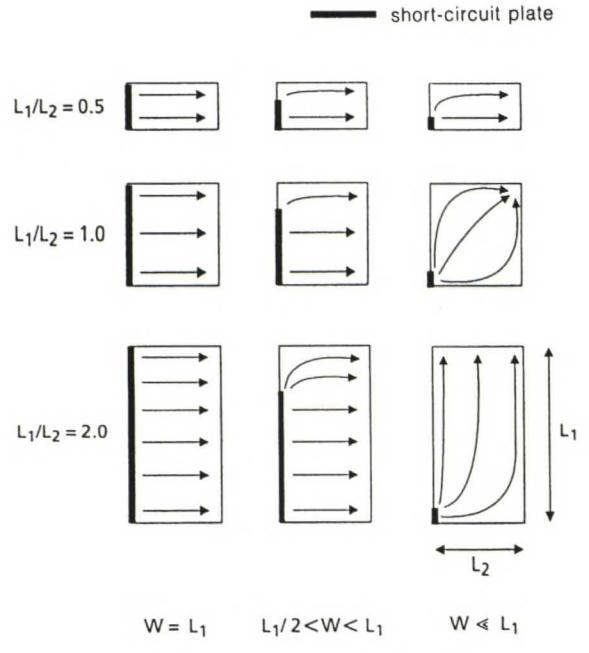

Figure 3.6 *Variation of surface current flowing on radiating plate due to size ratio of radiating plate and width of short circuit plate [28]. Here, L_1 is the width and L_2 is the length of the radiating plate, and W is the width of the short circuit plate.*

Variation of resonant frequency versus width of short circuit plate is illustrated in Figure 3.7. As a rule the resonant frequency decreases when the width of the short circuit is reduced.

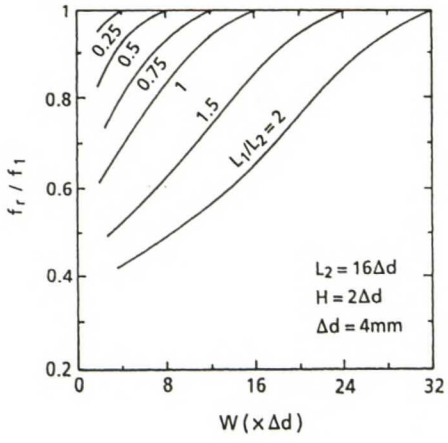

Figure 3.7 *Variation of resonant frequency versus width of short circuit plate [28]. Here, L_1 is the width and L_2 is the length of the radiating plate, and W is the width of the short circuit plate. The resonance condition for frequency f_1 is expressed by Equation (3.14).*

In Section 3.2.2, Equations (3.14) and (3.15) were presented for resonant condition for special cases where the short circuit width w is equal to radiating plate width W or equal to zero. In general case, when $0 < w/W < 1$, the resonant frequency of a PIFA can be calculated according to the following equations [28]:

$$f_r = r \cdot f_1 + (1-r) \cdot f_2 \quad for \ \frac{W}{L} \leq 1 \tag{3.16}$$

$$f_r = r^k \cdot f_1 + (1-r^k) \cdot f_2 \quad for \ \frac{W}{L} > 1 \tag{3.17}$$

where $r = w/W$, $k = W/L$, resonance condition for frequency f_1 is expressed by Equation (3.14) and resonance condition for frequency f_2 by the following equation:

$$W + L + h - w = \frac{\lambda}{4}. \tag{3.18}$$

The fringing fields at open-circuited edges are the dominating radiating sources in PIFAs. The radiation pattern depends strongly on the size and shape of the ground plane

on which the antenna is mounted and also on the antenna position on the conducting emplacement.

3.2.4 Loss mechanisms and quality factors

For an effective antenna operation, a PIFA should have the radiation loss as large as possible, i.e. the radiation quality factor as small as possible.

Dielectric material can be used as a substrate of a PIFA but the lossy substrate material lowers the radiation efficiency. The calculation of dielectric losses can be specified in terms of loss tangent using Equation (2.10) [30]. However, by a proper material choice, these are typically very small losses.

The conductor loss generally dominates over the dielectric loss. The quality factor for conductor losses of the radiating plate and the ground plane can be stated as [30]

$$Q_c = h\sqrt{\pi f_r \mu_0 \sigma_c}\,, \tag{3.19}$$

where μ_0 is the permeability in vacuum and σ_c is conductivity. Most often copper is used as the radiating plate and the ground plane material. Due to surface roughness, the effective conductivity of the copper is usually taken to be approximately $\sigma_c = 3 \cdot 10^7$ S/m rather than that of a pure bulk material ($\sigma_c = 5.8 \cdot 10^7$ S/m) [31]. It should be noted that Equation (3.19) does not contain the fact that the fields are not totally between the radiating plate and the ground plane but they are partly in the air. In addition, the current distribution is assumed uniform and the losses of the other metallic parts than the radiating plate and the ground plane (e.g. antenna feed and short circuit) are excluded. Accordingly, Equation (3.19) holds more accurately in the case of a wide radiating plate.

3.2.5 Bandwidth

The bandwidth of a PIFA is relatively large considering small antennas. The antenna height is the dominant factor which determines the bandwidth. Bandwidth of a PIFA increases with an increase in height like the bandwidth of microstrip antennas. Bandwidth of a PIFA as a function of antenna height in wavelengths (h/λ_0) is presented in Figure 3.8a for different *W/L*-ratios when $w = W$, and in Figure 3.8b for different *w/W* ratios when $W = L$. As shown in Figure 3.8, bandwidth increases with an increase in relation *W/L* (plate *width/length*) and decreases when reducing the width of the short circuit plate.

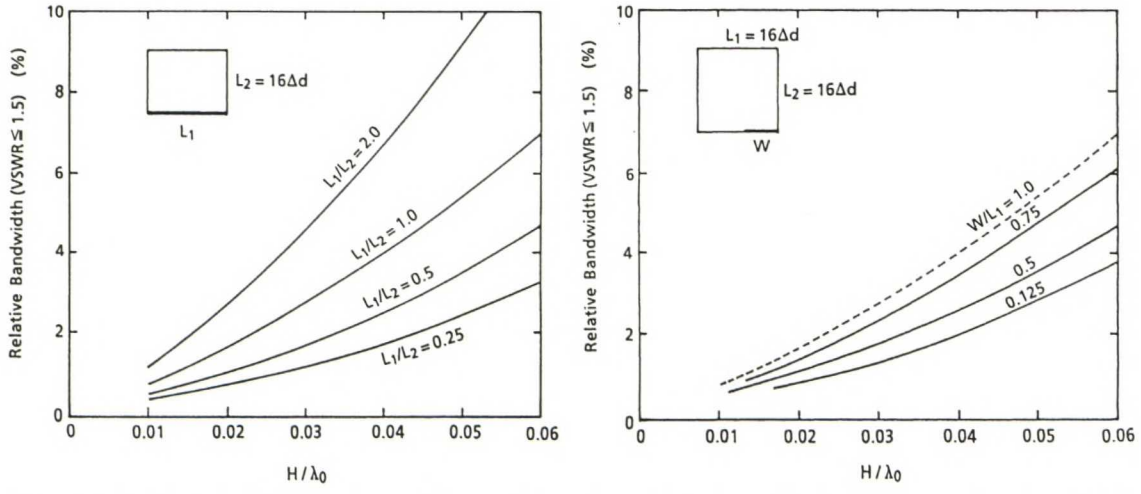

Figure 3.8 *Bandwidth of the PIFA as a function of antenna height in wavelengths [28]. Here, L_1 is the width and L_2 is the length of the radiating plate, and W is the width of the short circuit plate.*

a) The short circuit plate width is equal to radiating plate width (the case of short circuit MSA).

b) The short circuit plate width is narrower than the radiating plate width.

Reducing the ground plane size, the bandwidth can be broadened; the bandwidth of a PIFA mounted on a handset model is wider than that of a PIFA on an infinite ground plane because of the surface current flowing on the conductive emplacement [28].

3.2.6 Overview of feeding methods

Various excitation methods are applied for planar inverted F antennas. The most common, practically a standard feeding method for a PIFA, is excitation by a probe.

Other typically used feeding methods are capacitive feed [32], aperture feed [33], and electromagnetic coupling [34].

A feed probe is generally constructed from a coaxial cable. The inner conductor of a coaxial line is connected into the radiating plate and the outer connector is connected into the ground plane (see Figure 3.5). In order to match the feed probe to the antenna input impedance, the probe has to be properly positioned. Near the short circuit, the probe impedance is close to zero. It increases as the probe is moved closer to the radiating edge. Typically, the location is selected at the edge of the radiating plate because of easier practical implementation. For thicker antennas this excitation method introduces a significant series reactance due to extension of the feed probe.

The probe inductance can be canceled out by using capacitive feeding. A capacitive feed, also known as noncontact feed, can be implemented by terminating the inner conductor of a coaxial with a conducting plate, which will couple electromagnetically into the radiating element (see Figure 3.9). Adjusting can be made by changing the size of the feed plate, the distance between the feed and the radiating plate and the location of the feed.

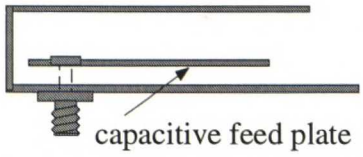

Figure 3.9 *Capacitive feed arrangement of a PIFA.*

Excitation of a PIFA by aperture coupling is accomplished by coupling the fields of a microstrip line feed on one substrate to a PIFA on another substrate through an electrically small aperture in the ground plane separating the two substrates. The aspects regarding the aperture size, and the advantages as well as the disadvantages of the method were already discussed when DRA excitation by aperture coupling was introduced (see Section 3.1.6).

PIFAs can also be fed by electromagnetic coupling (also proximity coupling). In that, both the radiating plate and the microstrip transmission line (feed) share the same substrate and the same ground plane. Typically the feed line is buried in the substrate between the ground plane and the radiating plate. The main advantages of this excitation method are reduced spurious radiation from the feed and the easiness of integration.

4 Miniaturization methods

Some suitable candidates for integrated antennas were introduced in Chapter 3. As such, they are still considered too large for practical handset applications and there is a need to reduce the overall size of the antenna. As was described in Chapter 2, the antenna size is strongly linked into the resonant frequency, the quality factors, and the radiation efficiency. Typically, the smaller the antenna size relative to the operating wavelength is, the larger the Q_0-value grows (resulting in a narrower bandwidth), and the lower the antenna efficiency turns [4]. The primary aim is, however, at effective small-sized broadband antennas. By finding the means for downsizing an antenna without sacrificing the performance, the resulting miniaturized antenna would be compatible to that needed in the future handset terminals.

When competently miniaturizing an antenna, the resonant frequency remains the same even though the antenna size is reduced. Actually miniaturizing can be considered also as a decrease in the resonant frequency while preserving the antenna size, i.e. the resonant condition is met at a lower frequency. There are several means for miniaturization. More than one techniques may be used simultaneously. Typically downsizing can be accomplished:

- by strategically placing a metallic plane into an antenna system, and then utilizing image theory to remove half of the antenna structure while preserving the proper mode configuration.

- by loading the antenna in a way that the self-resonance is obtained when the antenna volume is smaller than that of a conventional structure. The antenna can be loaded dielectrically, reactively, or resistively.

- by increasing the effective resonator length by bending the structure according to some geometrical configuration.

In this chapter these different miniaturization techniques are presented. At first, a description of the theoretical principles on each method is given. Then a practical approach is taken applying the techniques to the antenna types presented in Chapter 3.

4.1 IMAGE METHOD

4.1.1 Principles

According to image theory, the conducting plane can be removed when placing current sources, i. e. a mirror image on the other side of the plane in a way that the tangential component of the field created by an antenna and the mirror image disappears at the plane. Virtual sources are presented to account for the reflections from the metallic plane [11].

By applying image theory inversely, half of the antenna structure can be replaced by an image by strategically placing a metallic plate into an antenna system where a certain field symmetry exists. The location of an added metallic plate has to be in a plane of symmetry in the E-fields and in a place where the electric field component tangential to the added plate does not exist. The plate should be assumed to be a perfect electric conductor (PEC) and infinite in size; then the reflection from the conducting plane is complete and image theory is valid.

Applying a short circuit into an antenna structure approximately halves the antenna size. Theoretically the field distribution and the resonant frequency are preserved. In practice, some variations can appear since the added metallic plate is not ideal. This equivalent

system gives the same radiated field above the metallic plate as the actual system itself. Below the conductor the equivalent system does not give the correct field; in an ideal case with an infinite size PEC-plate the field is actually zero.

4.1.2 Dielectric resonator antennas

Actually all practical DRAs reported until now have been located on a conducting plane and hence have had height of half that of the isolated dielectric resonator [19]. A novel research issue concerns further reducing the size of a conventional DRA by employing an additional metallic plate perpendicular to the ground plane on which the resonator is placed [17, 35]. This additional plate acts also as an electrical wall and allows half of the structure to be removed if certain field symmetry exists (see Section 4.1.1).

As already mentioned in Chapter 3, the lowest order mode excited in the rectangular resonator is $TE^{z}_{11\delta}$ if the dimensions of the DRA are such that $a > b > d$. The fields of that mode are presented in Figure 4.1a. In Figure 4.1b an equivalent structure to Figure 4.1a is illustrated. The structure in Figure 4.1b is called a half-volume DRA (HV-DRA).

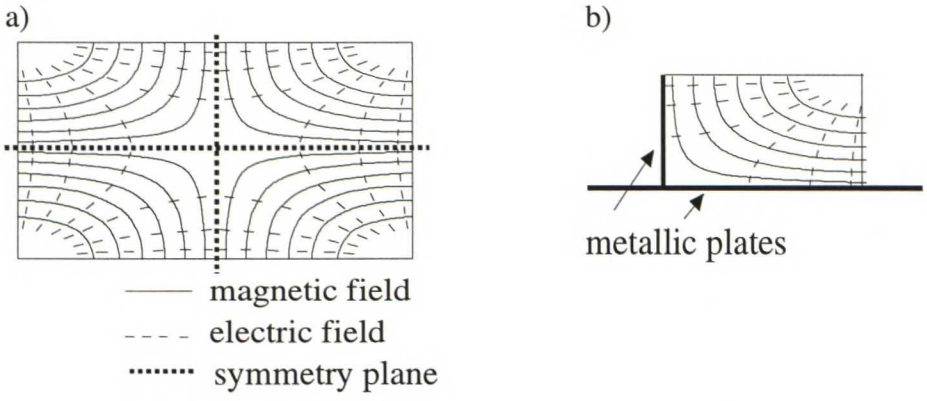

Figure 4.1 *a) Electric and magnetic fields of $TE_{11\delta}$-mode inside an isolated rectangular dielectric resonator, side view. b) HV-DRA.*

Downsizing a DRA with a perpendicular metallic plate leads to an increase in the conducting parts of the antenna, which in turn causes higher conductor losses. Further, the conductor losses induced in the metallic plate degrade the radiation efficiency compared to a conventional structure. Also the impedance characteristics are changed.

Hence the position and size of the feed have to be adjusted to obtain a match in a half-volume structure [35]. In addition, variations in quality factors may take place compared to a full-sized structure, even though the amount of the stored energy inside the resonator as well as the radiating surface (and thus the power radiated by the structure) are theoretically reduced by half.

4.1.3 Planar inverted F antennas

In fact, a PIFA with a full-width short circuit is equivalent to an air-filled short-circuited microstrip antenna, also called a λ/4-microstrip antenna. The short circuit introduced across the center of the patch of a λ/2-antenna allows the resonant length to be reduced by a factor of two for a given resonant frequency.

4.2 MATERIAL (DIELECTRIC) LOADING

4.2.1 Principles

Most of the conventional planar printed-circuit antennas are made of materials of low relative permittivity ($\varepsilon_r' < 10$) [36]. Nevertheless, the wavelength in the resonator material depends on the relative permittivity value according to Equation (3.1). Consequently, dielectric loading allows the element size to be reduced for a given operating frequency.

The relative permittivity cannot be chosen too high, otherwise radiation will be suppressed as more energy is stored in the material. Due to the decreased radiation, the radiation efficiency typically decreases with an increase in the relative permittivity value as does the antenna gain [4, 37]. Also decrease in the impedance bandwidth with increased ε_r' has been reported [4,16].

4.2.2 Dielectric resonator antennas

In a DRA the high permittivity value ensures that most of the fields are contained within the dielectric. When all the antenna dimensions are scaled down with $\sqrt{\varepsilon_r'}$, the size of the radiating aperture decreases. Since field fringing and leakage from the sides enables antenna operation, the radiated power is smaller in high permittivity resonators. The radiation quality factor values of rectangular DRAs radiating like magnetic dipoles depend on the relative permittivity value approximately according to Equation (3.11). Hence, an increase in the relative permittivity value increases radiation quality factor and accordingly reduces bandwidth and radiation efficiency of DRAs [22]. In addition, metallic losses of certain types DRAs become larger with increased ε_r' according to Equation (3.13).

It is concluded in [38] that a dielectric resonator with low relative permittivity is preferred for constructing the antenna due to the wider impedance bandwidth and easier impedance matching. Nevertheless, the value of ε_r' cannot be chosen very small, otherwise the radiation quality factor may become too small and will adversely affect the amplitude of fields for the resonant mode, and therefore the radiation characteristics [39]. With a very low value of material relative permittivity there does not exist a proper resonance.

4.2.3 Planar inverted F antennas

A miniature PIFA can be constructed by filling a conventional PIFA with high permittivity material (see Figure 4.2). The loading, however, decreases the bandwidth and radiation efficiency [40]. The radiation loss due to dielectric loading can be partly overcome by adding a very high permittivity layer (superstrate) on the radiating plate [36, 40].

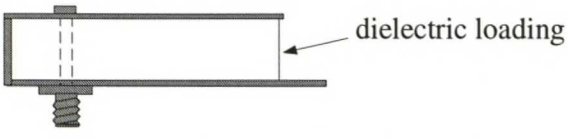

Figure 4.2 *Dielectrically loaded PIFA.*

A planar inverted F antenna can also be filled partially with a dielectric material or the dielectric loading between the radiating plate and the ground plane may be implemented using several materials of different relative permittivity value.

4.3 REACTIVE LOADING

Near its fundamental resonance any small antenna can always be modeled as an equivalent resonant circuit (see Figure 2.1). The resonant frequency of an equivalent RLC lumped element circuit is decreased when a capacitor or inductor is added in parallel with the circuit since the resonant frequency can be written as

$$f_r = \frac{1}{2\pi\sqrt{LC}}. \tag{4.1}$$

Therefore strategically placed loads can reduce the antenna size by lowering the resonant frequency. The amount of change in the resonant frequency depends upon the load value and the loading position. Using purely reactive load consumes no power. Different reactive loading techniques can be easily applied to PIFAs.

4.3.1 Inductive loading

The most common technique for miniaturizing a PIFA is inductive loading. It is implemented by fabricating the short circuit plate narrower than the radiating plate. The short circuit introduces inductance to the circuit [30]. Hereby the effective length of the current flow on the radiating plate and short circuit plate increases and the resonant frequency becomes lower [28]. The reduction in the short circuit width increases the loading inductance and decreases the resonant frequency. When placing the short circuit plate at the corner of the radiating plate, the resonant frequency is lower compared to the case when the short circuit is in the middle of the plate edge [28].

4.3.2 Capacitive loading

By adding a capacitive load to a PIFA, the resonant frequency can be reduced by any desired amount but at the expense of operating bandwidth and good matching [41]. The capacitive load of a PIFA can be formed by folding the open end of the top plate towards the ground plane. Moreover, a parallel plate between the top and the ground plane can be added.

The resonant frequency is controlled by the size of the capacitive load. The capacitance value can be increased by decreasing the distance between the capacitance and the ground plane or making the capacitive plate longer as the capacitance value is obtained from the equation:

$$C = \frac{A}{d_{CAP}} \varepsilon_0 \varepsilon_r' . \tag{4.2}$$

Here, A is the area of the capacitive plate, d_{CAP} is the distance between the capacitance and the ground plane, ε_r' and ε_0 are parameters for the material between the capacitor plates [42].

To improve the impedance characteristics of a capacitively loaded PIFA, a capacitive feed arrangement may be utilized [41, 43]. Manipulation of the impedance curves is possible by adjusting the feed plate area and its separation from the top plate and probe placement on the feed plate [32]. In addition, the capacitive feed plate can be made to resonate, and this dual resonant-structure partially compensates the bandwidth degradation due to the capacitive load. Structure of a capacitively fed and loaded PIFA is presented in Figure 4.3.

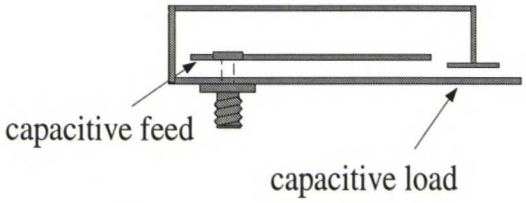

Figure 4.3 *Capacitively fed and loaded PIFA.*

A capacitively loaded PIFA is expected to have slightly lower efficiency than that of a conventional PIFA [41]. The reason can be found from the different current distributions. In a capacitively loaded PIFA the current distribution on the top plate is more uniform and larger in magnitude than in a conventional PIFA due to the capacitive load. Also the current flowing on the capacitive feed plate will add to the losses.

4.4 RESISTIVE LOADING

Instead of using a short circuit on the edge of a resonator, a chip resistor of low resistance can be utilized [44, 45]. As the resistive load absorbs power, a wider bandwidth can be obtained compared to a short circuit structure (see Figure 2.2).

The radiating plate of a PIFA can be connected to the ground plane by a chip resistor as illustrated in Figure 4.4. This is reported to enhance the antenna bandwidth characteristics; the larger the load resistor is, the wider the obtained bandwidth becomes. However, the bandwidth enhancement occurs at the expense of the antenna gain due to the ohmic loss of the loading resistance [44].

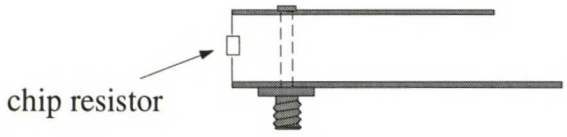

Figure 4.4 *Resistively loaded PIFA.*

If the location of the load is at the edge of the radiating plate, the maximum resonant frequency reduction can be achieved, as is the case with short circuit (see Section 4.3.1) [46].

4.5 SLOW WAVE STRUCTURES

A compact resonant antenna can be achieved through geometrical modification of the antenna structure. E.g. helical antennas can be made much shorter than monopoles as the effective length of the helical structure is greater than its physical length. Unfortunately, the bandwidth of these kind of structures if typically narrow [47].

A miniaturized PIFA can be accomplished by meandering (i.e. cutting several slits) the radiating plate so that the electrical length of the plate is increased and the plate is made to resonate at a lower frequency [44]. A meandered radiating plate is illustrated in Figure 4.5.

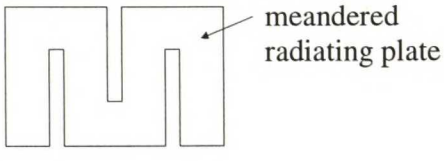

Figure 4.5 *Meandered radiating plate of a PIFA.*

The slits make the effective length of the current path longer; the top plate current flows around the slit creating an electrically longer antenna [48]. When the slit is made longer, the resonant frequency will decrease more. The width of the slit has no effect when the width is smaller than the height of the substrate. If the width is very small, the capacitance over the slit becomes significant [49].

5 Prototypes and measurements

Antenna performance cannot always be known by theory, but rather by experiment. To verify the validity of the theory presented in the previous chapters, size reduction techniques were applied in practice with prototype antennas. The selection of the developed prototype antennas was based on a fact that a comprehensive coverage of the theoretically presented miniaturization techniques (in Chapter 4) was obtained. Prototypes included a set of half-volume dielectric resonator antennas (HV-DRA) of different permittivity material (ε_r' = 2...70) but of the same geometrical shape. The chosen DRA prototypes show the effect of the relative permittivity value on antenna performance. Prototypes also included a set of differently miniaturized PIFAs. The implemented PIFA miniaturization techniques were inductive, capacitive, dielectric, and resistive loading, and a meandered radiating plate. The PIFA prototypes enable the comparison between different size reduction techniques.

Parameters of the developed antennas, including reflection coefficients, radiation efficiencies, quality factors, radiation patterns, and gains are reported in this chapter. At first general considerations about the measurements and result analysis are given. Then the measurement results are presented for DRAs and PIFAs, respectively. Finally there is a summary of the measurement results.

The development of completed handset antennas is not the main issue of this thesis. Instead, the main purpose of the work is to find out how different miniaturization techniques affect the antenna performance. Since a basic research of the general behavior of differently miniaturized antennas was needed, the prototypes were constructed on a

large ground plane, even though the characteristics of antennas on a large ground plane are usually different from those of antennas mounted on portable handsets. However, the actual antenna performance can hereby be investigated; no resonances or radiation effects of the handset itself need to be considered and a comfortable comparison between the prototype antennas is possible. The large ground plane also offers the advantage of an easy implementation of radiation efficiency measurements.

5.1 GENERAL MEASUREMENT AND ANALYSIS CONSIDERATIONS

5.1.1 Reflection coefficient measurement

The reflection coefficients of the antennas were measured with a vector network analyzer. In order to minimize the effect of reflections in the measurement room during the reflection coefficient measurement, the antennas were pointed at an absorbing material.

5.1.2 Efficiency measurement

Radiation efficiencies of the prototype antennas were measured with the Wheeler cap method (WCM) [5,19]. The method is based on a fact that if a metal cap is placed around an antenna enclosing the near fields of the antenna, the radiation resistance is reduced to zero. The other properties of the antenna, including the loss resistance and the stored energy, remain the same as for the uncapped case. When measuring the radiation efficiency with the WCM, it is assumed that when enclosing the antenna in a radiation cap, the current distribution on a small antenna remains. Actually, when the antenna is enclosed with a cap, the current distribution undergoes a small change and consequently the resonant frequency changes slightly. However, this frequency shift can be considered [50].

The procedure was to measure the antenna reflection coefficients at resonance with and without the cap. The measured results were used to calculate the respective input resistances [50]:

$$R_{in} = \frac{1 \pm |\rho_r|}{1 \mp |\rho_r|}. \tag{5.1}$$

Here, the upper signs are for the undercoupled and the lower signs for the overcoupled cases. Equation (5.1) is derived for a series resonant circuit.

The radiation efficiency is the ratio of the radiated power and the input power as expressed in Equation (2.17). The efficiency can also be written using input resistances:

$$\eta_r = \frac{P_{rad}}{P_{in}} = \frac{R_r}{R_r + R_l} = \frac{R_{uncap} - R_{cap}}{R_{uncap}}, \tag{5.2}$$

where R_r is radiation resistance, R_l is loss resistance, R_{uncap} is the input resistance of the antenna without the cap, and R_{cap} is the input resistance of the antenna with the cap.

The measurements were repeated with several caps of different size, shape, and material. There are general requirements for the properties of the caps. The cap shape may be arbitrary but an overall minimum size restriction could be stated for the cap radius; it must be larger than one radianlength $\lambda_0/2\pi$ in order that the cap edge is outside the near field region of the antenna [51]. If the cap size is too small, i.e. the cap edges are too close to the antenna, obvious changes in the antenna current distribution take place when compared to the isolated case. On the other hand, if the cap size is too large, the resonances of the cap itself (cavity resonant modes) start to disturb the measurement. The finite conductivity of the cap does introduce conductor losses. However, current density on the cap is small due to the large area of the cap, and the loss can be considered negligible if the cap is constructed of a high-conductivity material.

In the implemented measurements the cap materials used were copper, aluminum, and gilt steel. The radius of each cap was larger than a radianlength. Still, the cap sizes were

small enough not to excite a cavity resonance at the same frequency as the actual resonant frequency of the antenna. Hence the criteria of high-conducting material as well as reasonable size were fulfilled.

5.1.3 Quality factor analysis

Quality factor analysis was made based on the reflection coefficient and radiation efficiency measurements. At first the loaded quality factor was calculated from the measured resonant frequency f_r and half power bandwidth B_{HP} [1]:

$$Q_L = \frac{f_r}{B_{HP}}. \tag{5.3}$$

B_{HP} was taken between the points in which the power reflection coefficient had fallen halfway from the maximum value of 0 dB to the minimum value, i.e. between the points in which the power reflection coefficient was

$$|\rho|^2 = \frac{1+|\rho_{\min}|^2}{2}. \tag{5.4}$$

Unloaded quality factor Q_0 was then calculated according to Equation (2.7).

Radiation quality factor Q_r was obtained from Equation (2.17) after the radiation efficiency measurement.

When the antenna is uncapped, Q_0 can be expressed according to the following

$$\frac{1}{Q_0} = \frac{1}{Q_{cd}} + \frac{1}{Q_r}, \tag{5.5}$$

where Q_{cd} is the quality factor of dielectric and conductor losses. It was assumed to remain the same for the uncapped and capped cases as the cap material and size criteria were fulfilled (see Section 5.1.2).

Since the power loss occurs both in the dielectric and the conductors, the contributions of dielectric and conductor quality factors Q_d and Q_c were estimated. The estimation was based on an approximation that the fields were totally inside the resonator (see Section 2.1.3). Therefore the calculation of Q_d was made according to Equation (2.10). The rest of the losses were assumed to be due to imperfect conductor material.

5.1.4 Radiation patterns

The radiation patterns of the antennas were also studied. The measurements were carried out in the anechoic chamber of HUT. The measurements were implemented in the receiving mode and a horn antenna (model H-5001 manufactured by AEL Industries, Inc.) was used as a transmitter. Some parameters of the transmitter horn antenna are presented in Table 5.1. The measured reflection coefficient as a function of frequency for the transmitter antenna is presented in Figure 5.1.

Table 5.1 *Parameters of the transmitter horn antenna.*

Frequency [GHz]	Nominal gain [dBi]	3 dB beamwidth E-plane [degrees]	3 dB beamwidth H-plane [degrees]
1.0-2.5	15	30	35

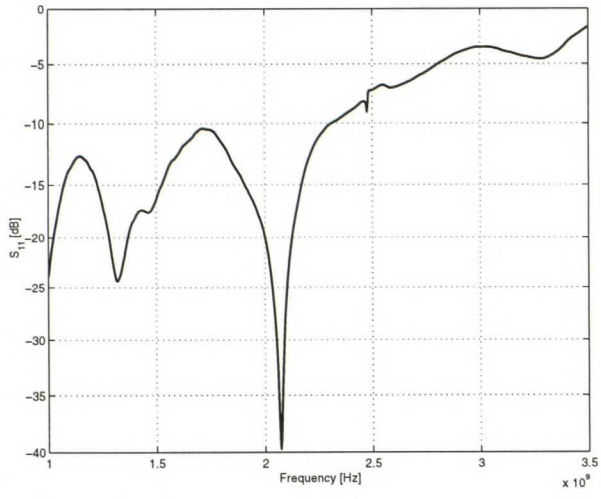

Figure 5.1 *The measured reflection coefficient as a function of frequency for the transmitter antenna.*

The receiver antenna was rotated in azimuth (ϕ) and elevation (θ) planes and two pattern cuts were measured when the network analyzer was connected to the Flamm & Russell FR959 Antenna Measurement Workstation. The radiation patterns are given in polar form since they provide a better visualization of the radiation distribution of the prototypes than linear plots. All patterns of the certain prototype antenna were normalized to the same received maximum power level. Orientation of the receiver antenna during the radiation pattern measurements is shown in Figure 5.2. The corresponding axes are marked into the polar plots. The transmitter horn was located in the x-axis 3.75 meters away from the receiver.

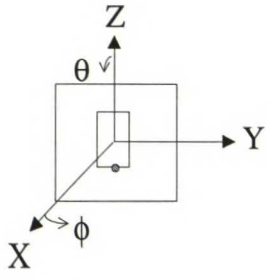

Figure 5.2 *Orientation of the receiver antenna in radiation pattern measurements. The dot shows the direction of the short-circuit.*

5.1.5 Antenna gains

The antenna gains were measured using gain comparison. This measurement was also performed in the anechoic chamber of HUT. The same transmitter horn was used as in the radiation pattern measurements. Using the prototype antennas as receiving antennas, the transmission coefficient S_{21} was recorded by a vector network analyzer. The receiver antenna was then replaced by a reference antenna and S_{21} was recorded. The geometrical arrangement and the input power were maintained the same (other than replacing the receiving antennas).

Due to the unknown self-calibration of the network analyzer by the radiation pattern measurement software, the gain measurement was not performed simultaneously with the radiation pattern measurement. Instead, for the gain measurement, a proper calibration was done in order to obtain more accurate results. The measurement cables were included in the measurement calibration so that the measured S_{21} corresponded

directly to the S_{21} from the connector of the transmitting antenna to the connector of the receiving antenna.

A double-ridged horn antenna (model BBHA 9120-A2 manufactured by Schwarzbeck - Mess Elektronik) was used as a reference receiver antenna. The gain values of the horn at several frequencies were provided by the manufacturer. The graph of the gain was plotted according to those and is presented in Figure 5.3. The measured reflection coefficient is presented in Figure 5.4.

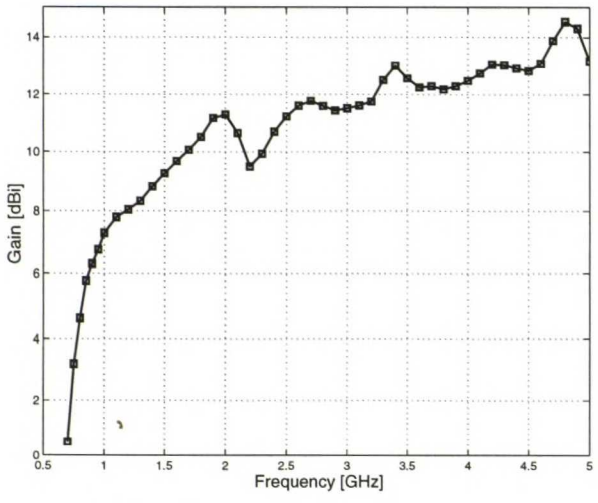

Figure 5.3 *Reference horn antenna gain as a function of frequency.*

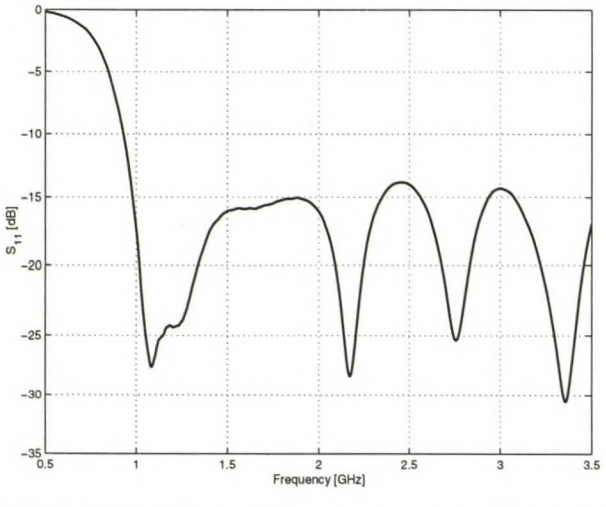

Figure 5.4 *Reference horn antenna reflection coefficient as a function of frequency.*

The gains of the prototype antennas G_{proto} could be obtained with the known reference antenna and the measured transmission coefficient values:

$$G_{proto} = \frac{S_{21,proto}}{S_{21,ref}} \cdot G_{ref}, \tag{5.6}$$

where $S_{21,proto}$ is the measured transmission coefficient using the prototype, $S_{21,ref}$ is the measured transmission coefficient using the reference antenna, and G_{ref} is the gain of the reference antenna. The values were measured only for E_θ - polarization in the direction of the x-axis and then scaled to the direction of the maximum power gain according to the radiation pattern measurements. Due to the improper matching of the prototypes, the gain values were finally corrected according to the reflection coefficient value in antenna feed, i.e. including the reflection loss into the gain definition (see Section 2.1.5).

5.2 DIELECTRIC RESONATOR ANTENNAS

5.2.1 Antenna structures and construction

To study the impact of relative permittivity on dielectric resonator antenna performance, rectangular HV-DRA prototypes were constructed from five kinds of dielectric materials. The antenna presented in [35] was selected as the basis for the antennas realized here. The resonator dimensions were approximately scaled according to the relative permittivity value in order to keep a fixed geometrical shape. The material parameters and the antenna dimensions are listed in Table 5.2.

The antenna configuration is shown in Figure 5.5. The resonator element was placed symmetrically and glued to a 150 mm by 150 mm ground plane using acrylat glue. The copper ground plane had a thickness of 1 mm. Short circuit plate perpendicular to the ground plane was glued to the edge of the element and soldered to the ground plane. The short circuit plate was also made of copper. It had a thickness of 0.3 mm. The antenna was excited by an extended inner conductor of an SMA connector inserted from beneath the ground plane into the dielectric. The feed position was selected in the middle of the resonator in order to achieve the strongest coupling as the $TE^{z}_{11\delta}$ -mode was excited (see Figure 4.1).

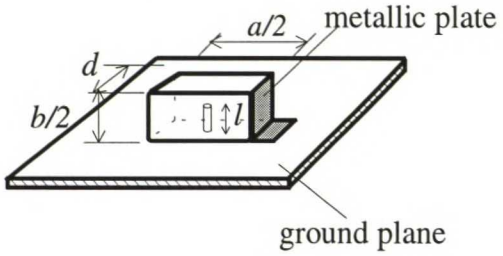

Figure 5.5 *Structure of a half-volume DRA prototype.*

Table 5.2 *Parameters of the half-volume DRA prototypes.*

ε_r'	**2.1**	**6.15**	**16**	**38**	**70**
tanδ	$3.0 \cdot 10^{-4}$	$2.5 \cdot 10^{-3}$	$7.0 \cdot 10^{-4}$	$2.6 \cdot 10^{-4}$	$6.9 \cdot 10^{-4}$
***a*/2 [mm]**	49.5	28.6	17.5	11.4	8.4
***b*/2 [mm]**	45.0	26.0	15.9	10.3	7.6
***d* [mm]**	22.0	12.6	8.0	5.2	3.8
***l* [mm]**	24.9	14.4	8.8	5.7	3.3

The antenna construction was inconvenient as the materials of higher permittivity value were so hard that they were difficult to process. In the consequence of this, the resonator elements of two DRAs with the highest permittivity values ($\varepsilon_r' = 38$ and $\varepsilon_r' = 70$) were constructed at Ylinen Electronics. The rest of the prototypes could be built with the equipment of the Radio Laboratory.

Only flat, thin pieces of materials of dielectric permittivity values $\varepsilon_r' = 6.15$, $\varepsilon_r' = 38$, and $\varepsilon_r' = 70$ were available. Therefore these resonator blocks were fabricated by glueing several plates one on the other using epoxy glue. The glue layers were made as thin and as even as possible.

A hole was drilled into the middle of the resonator for probe accommodation. This created a small air gap between the probe and the body of the DRA. Besides, even though the DRA elements were glued to the ground plane, there was an imperfect mechanical contact between the dielectric resonator and the conducting surface on which it resided. Hence there existed a thin air gap also between the ground plane and the dielectric block. These air gaps introduce discontinuities in the normal component of electric fields at the dielectric - air interfaces. This has effect on antenna performance [52].

5.2.2 Reflection coefficients

The measured reflection coefficients as a function of frequency for the HV-DRAs with $\varepsilon_r' = 2.1$, $\varepsilon_r' = 6.15$, $\varepsilon_r' = 16$, $\varepsilon_r' = 38$, and $\varepsilon_r' = 70$ are presented in Figure 5.6, respectively.

a) $\varepsilon_r' = 2.1$

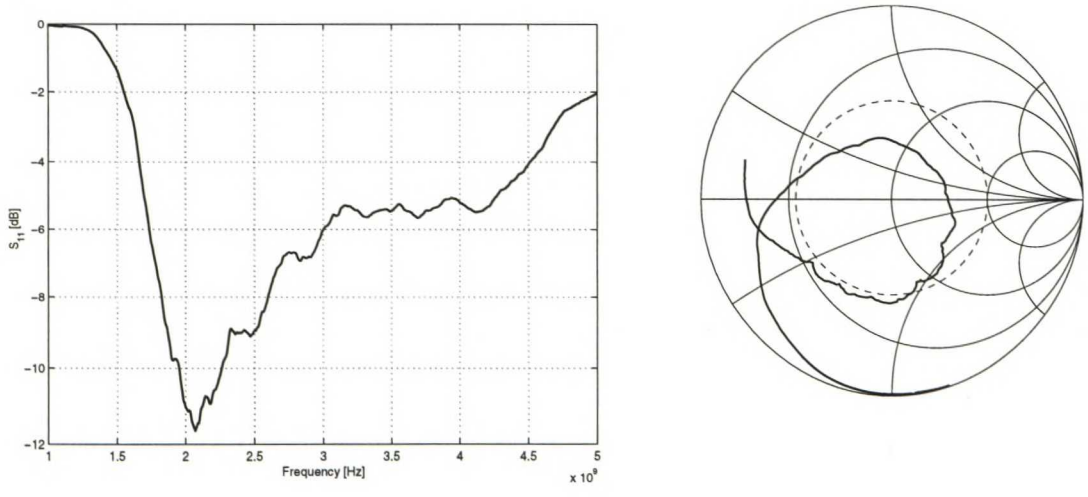

b) $\varepsilon_r' = 6.15$

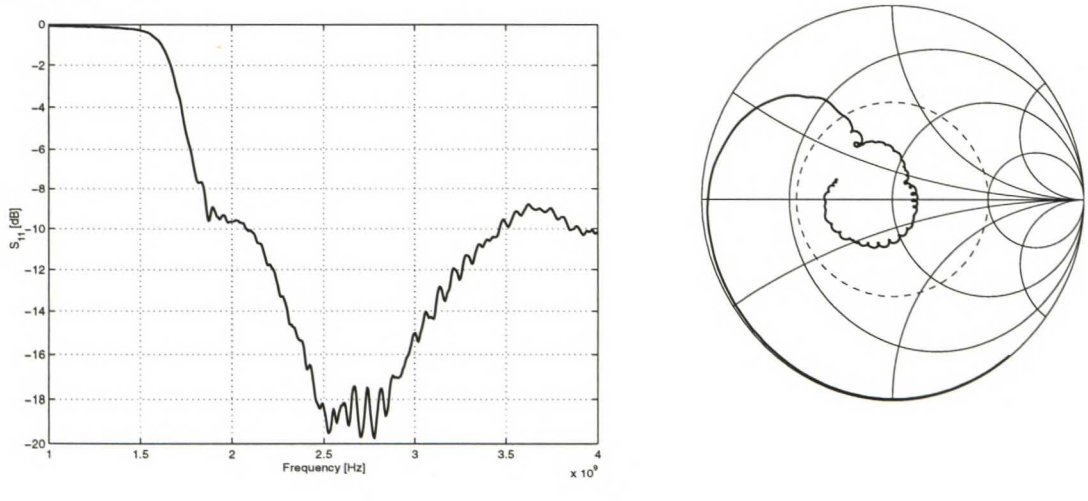

c) $\varepsilon_r' = 16$

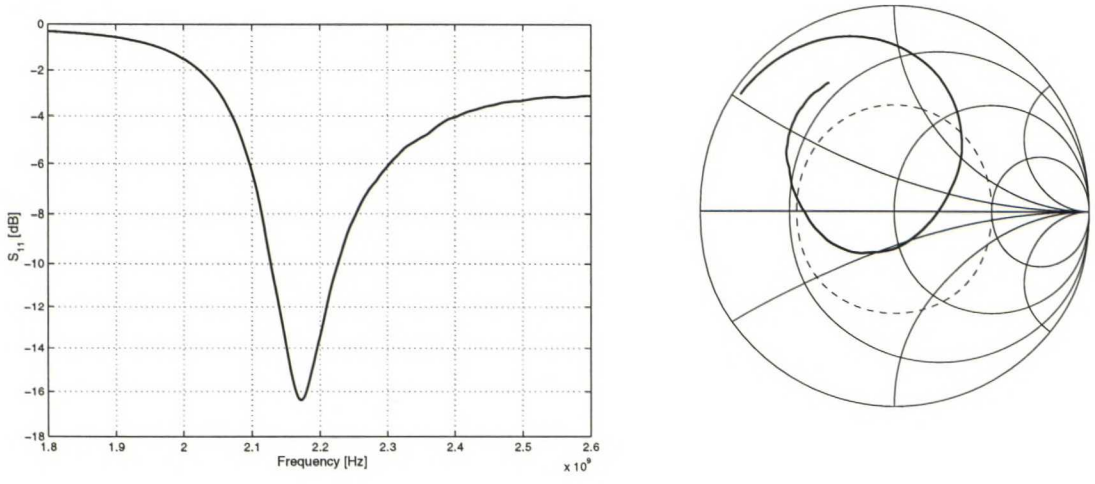

d) $\varepsilon_r' = 38$

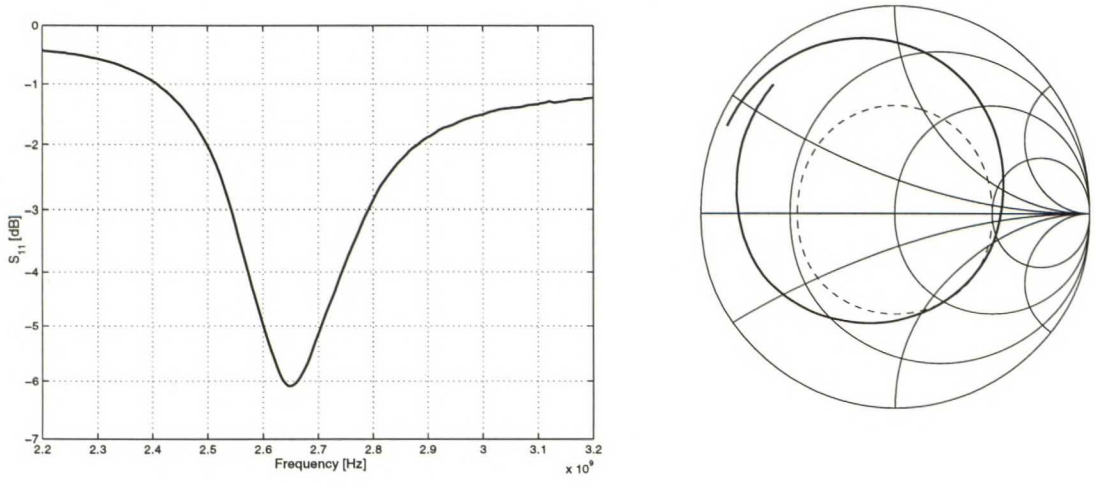

e) $\varepsilon_r' = 70$

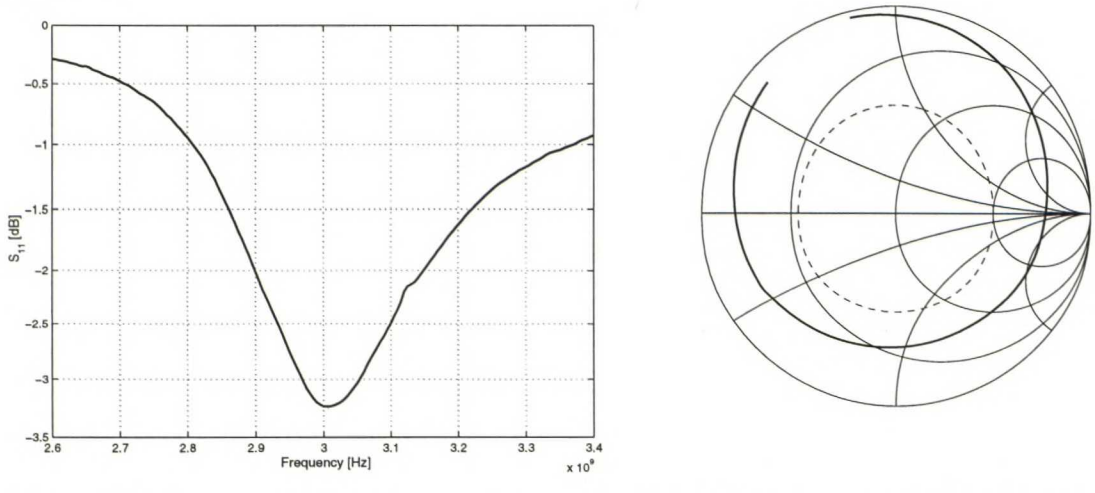

Figure 5.6 *Measured reflection coefficients for the HV-DRAs with a) $\varepsilon_r' = 2.1$, b) $\varepsilon_r' = 6.15$, c) $\varepsilon_r' = 16$, d) $\varepsilon_r' = 38$, e) $\varepsilon_r' = 70$. Dashed line represents the reflection coefficient $|\rho| = 0.501$ (L_{retn}= 6 dB).*

As Figures 5.6a and 5.6b show, no proper resonance could be found for the antennas with $\varepsilon_r' = 2.1$ and $\varepsilon_r' = 6.15$. In them, the relative permittivity value was probably too small for the structure to behave like a dielectric resonator antenna. It was assumed that the relative permittivity value of $\varepsilon_r \approx 10$ would be the lowest reasonable value. Due to the unclear resonant characteristics an approximative approach was taken when these two structures were analyzed.

The prototypes with $\varepsilon_r' = 38$ and $\varepsilon_r' = 70$ were not well matched which can be seen from Figures 5.6d and 5.6e. However, further adjustment of the feed was not possible because of the antenna structure and the feed arrangement.

Measured and theoretical resonant frequencies for the HV-DRAs are given in Table 5.3. The theoretical resonant frequencies were calculated according to Equations (3.3)-(3.6). As can be seen, the real operating frequencies of the prototypes were clearly different from the theoretical ones. This was assumed to result partly from the unideal short circuit plate in the half-volume structures. On the other hand, the theoretical equations do not give very good predictions for the resonant frequencies of full-sized DRAs either [53].

Table 5.3 *Measured and theoretical resonant frequencies.*

ε_r'	**2.1**	**6.15**	**16**	**38**	**70**
$f_{r,\,measured}$ **[MHz]**	2075	2566	2172	2642	3005
$f_{r,\,theoretical}$ **[MHz]**	2076	2433	2506	2535	2551

5.2.3 Efficiency measurements

The measured radiation efficiency values for HV-DRAs are presented in Table 5.4. The results obtained with different caps agreed very well; the uncertainty was ± 1 percentage units.

Table 5.4 *Radiation efficiencies.*

ε_r'	**2.1**	**6.15**	**16**	**38**	**70**
η_r [%]	99±1	95±1	93±1	89±1	86±1

The efficiency is noted to decrease as a function of permittivity value. It results from the increased internal losses. The reasons for that are discussed in the quality factor analysis in the next subsection. Nevertheless, it is seen that the efficiency stays high also for high values of ε_r'.

5.2.4 Quality factor analysis

Experimental results for the quality factors are shown in Table 5.5. It should be noted that Q_0-values for the antennas with $\varepsilon_r' = 2.1$ and $\varepsilon_r' = 6.15$ were roughly approximated due to unclear resonance characteristics. Q_0 for the antenna with $\varepsilon_r' = 16$ was calculated by correcting the reflection coefficient curve symmetric (see Figure 5.6c). In this case the half power bandwidth $B_{HP} = 413$ MHz was estimated for the 2.91 dB - level.

Table 5.5 *Experimental results for the quality factors.*

ε_r'	**2.1**	**6.15**	**16**	**38**	**70**
Q_0	2.0	2.7	12.4	28.2	51.5
Q_r	2.0	2.8	13.3	31.7	59.9
Q_d	3333	400	1429	3846	1449
Q_c	213	93	202	274	492

The results in Table 5.5 show that the radiation quality factors for antennas with $\varepsilon_r' \geq 16$ are approximately inversely proportional to the volume of the resonator in wavelengths as could be expected [see Equation (3.11)].

Accurate values for the dielectric loss factor $\tan\delta$ were supplied by the manufacturer. Other than $\varepsilon_r' = 6.15$ materials had very low losses. Still, the relative dielectric losses also for the antenna with $\varepsilon_r' = 6.15$ were small due to the low unloaded quality factor.

The conductor quality factor of resonators of similar shape and resonant mode should typically behave as $Q_c \propto (f_r/\varepsilon_r')^{1/2}$ [see Equation (3.13)]. However, this is not the case with the results in Table 5.5 as Q_c increases when ε_r' increases. The reason for this is probably that for lower values of ε_r' the monopole-type resonant currents in the vertical metallic short circuit plate or the feed probe or both are high. This can be seen also in the

radiation pattern results presented in Section 5.2.5. Despite this, the proportional part of conductor losses is noticed to increase when ε_r' increases.

5.2.5 Radiation patterns

The normalized radiation patterns for the antennas with $\varepsilon_r' = 2.1$, $\varepsilon_r' = 6.15$, $\varepsilon_r' = 16$, $\varepsilon_r' = 38$, and $\varepsilon_r' = 70$ are given in Figure 5.7, respectively. The coordinate system is presented in Figure 5.2

a) $\varepsilon_r' = 2.1, f = 2075$ MHz

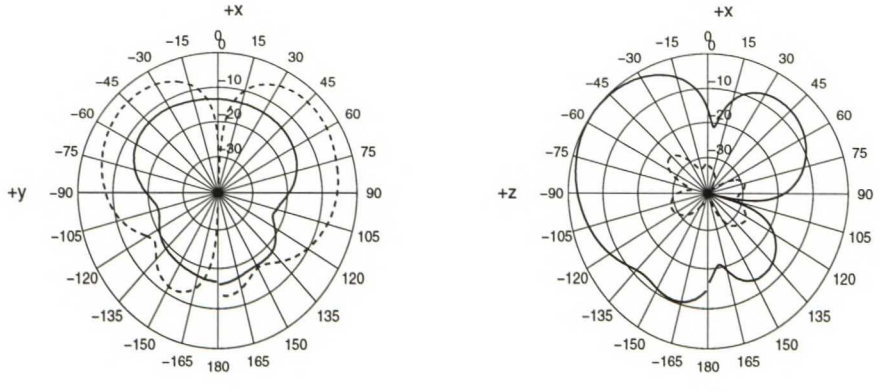

b) $\varepsilon_r' = 6.15, f = 2566$ MHz

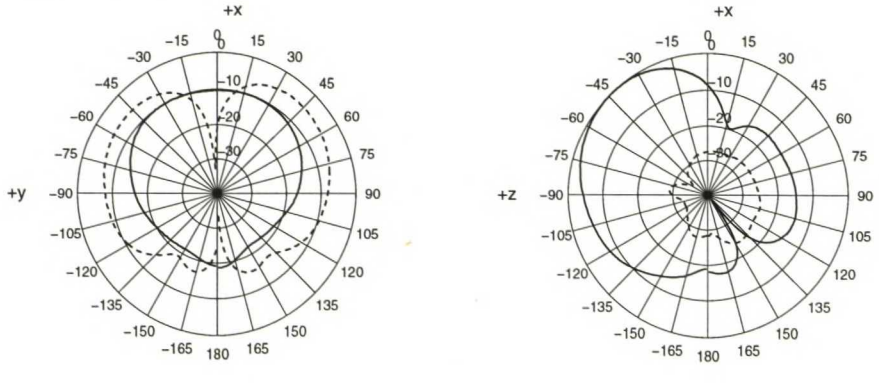

c) $\varepsilon_r' = 16, f = 2172$ MHz

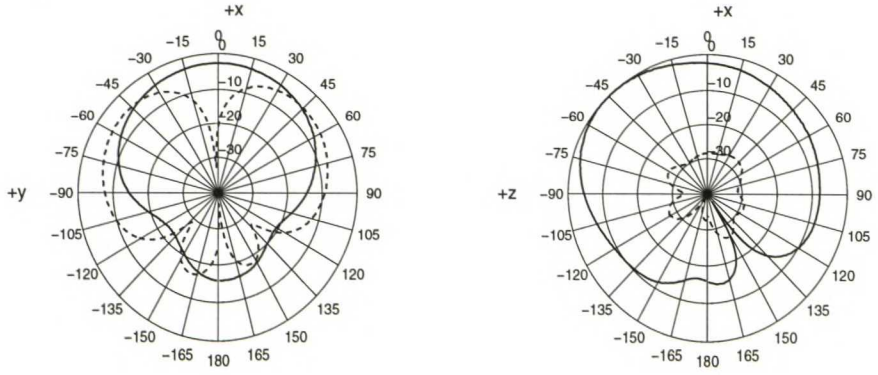

d) $\varepsilon_r' = 38, f = 2642$ MHz

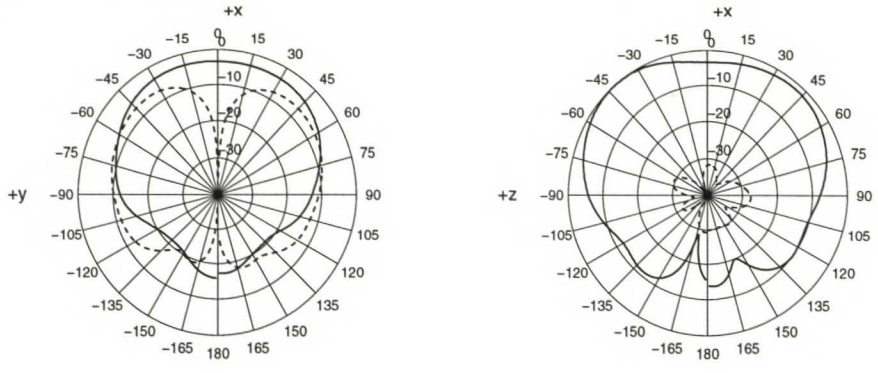

e) $\varepsilon_r' = 70, f = 3005$ MHz

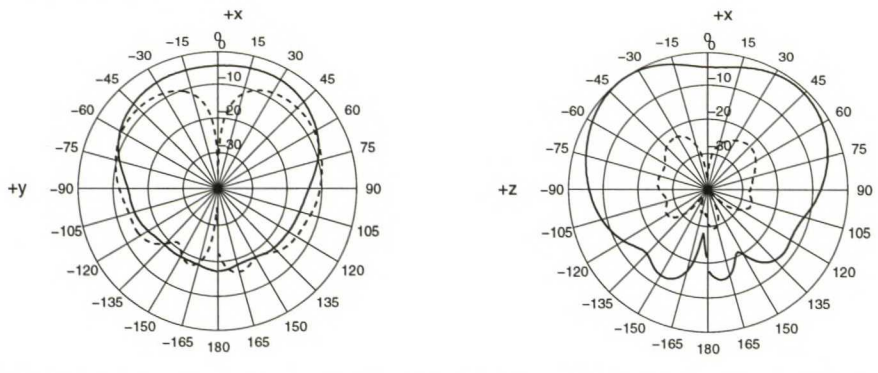

Figure 5.7 *Normalized radiation patterns for the HV-DRAs with a) $\varepsilon_r' = 2.1$, b) $\varepsilon_r' = 6.15$, c) $\varepsilon_r' = 16$, d) $\varepsilon_r' = 38$, e) $\varepsilon_r' = 70$. Solid line represents the E_θ - component and dashed line the E_ϕ - component.*

By comparing Figures 5.7a... 5.7e, it can be seen that the radiation patterns of the antennas with $\varepsilon_r' = 2.1$ and $\varepsilon_r' = 6.15$ resemble that of an (x-directed) electric dipole because of a high cross-polarization level in the xy-plane. In them, the radiation quality factor was assumed to have become too small and then adversely affected the amplitude of co-polarized fields for the resonant mode, and therefore the radiation characteristics.

The feed probe or the short circuit plate or both were considered to act as a small electric monopole and the direct radiation from those causes a high cross-polarization level. The radiation characteristics change gradually from that of an electric dipole to a (y-directed) magnetic dipole when increasing the permittivity value. The radiation patterns of the antennas with $\varepsilon_r' = 38$ and $\varepsilon_r' = 70$ resemble that of a magnetic dipole, as was expected [20]. Some asymmetry of the radiation pattern due to the short circuit plate can also be noticed.

5.2.6 Antenna gains

The measured antenna gains at resonant frequencies are given in Table 5.6. The gain values are considered to be relatively large. One reason for that is assumed to be in the large ground plane as when the antenna is placed on a large ground plane, its directivity theoretically increases by 3 dB compared to that of an isolated antenna since the power is radiated only in to one half-space. However, as can be seen from the radiation patterns (Figure 5.7), the radiation to the back of the ground plane was not entirely eliminated in practice.

Table 5.6 *Measured antenna gains.*

ε_r'	**2.1**	**6.15**	**16**	**38**	**70**
***G* [dB]**	7.8±1.1	6.2±1.1	5.6±1.1	5.8±1.1	5.2±1.1

It can be noticed from the results in Table 5.6 that the antenna with $\varepsilon_r' = 2.1$ has an exceptionally large gain value. As the gain values were measured only for the E_θ - polarization in the direction of the x-axis, a small misalignment of the antenna may have caused a large relative error in the gain (see Figure 5.7a). The gain decrease with increased ε_r' is mainly supposed to be due to the less directive pattern. The effect of a reduced η_r on gain is supposed to be small.

The limits of the uncertainty were approximated by considering the potential sources of uncertainty as was done in [54]. The uncertainty caused by the antenna room was approximated to be ±1 dB based on the measurements in [47]. The total uncertainty of

the network analyzer, the measurement cables and the alignment of the antennas was approximated to be ±0.5 dB. By squaring and summing the individual uncertainties and then by taking the square root of the sum, the total uncertainty of ±1.1 dB was obtained.

5.3 PLANAR INVERTED F ANTENNAS

5.3.1 Antenna structures and construction

In order to study the performance of different miniaturization methods, five differently miniaturized PIFA prototypes were constructed. A primary design criterion was to implement a PIFA of size 20mm × 10mm × 5mm. The antennas were designed to resonate at around 2 GHz.

Inductively, capacitively, and resistively loaded PIFA prototypes as well as the meandered PIFA were $\lambda/4$-resonators, i.e. their resonant length was reduced to half by introducing a short circuit at the edge of the resonator where the electric field was zero. The dielectrically loaded antenna was a $\lambda/2$-structure as a short circuit could not be added to this antenna; otherwise it would have had a resonant frequency approximately half of that of the other prototypes. Therefore the dielectrically loaded antenna was actually not a PIFA. However, in order to realize prototypes of the same physical size in the same frequency region, this structure was implemented as a $\lambda/2$-resonator.

All the tested PIFA prototypes were positioned symmetrically on a 150 mm by 150 mm copper ground plane of thickness 1 mm. As well, all PIFAs were built with the equipment of the Radio Laboratory.

Inductively loaded PIFA (PIFA)

Configuration of the inductively loaded PIFA is shown is Figure 5.8. The radiating plate of size $L \times W$ and of thickness t was short-circuited to the ground plane with a copper strip of width w and thickness t_{sc}. The short-circuit was located at the corner of the radiating plate. The distance between the short-circuit and the SMA feed probe was x.

The distance between the radiating plate and the ground plane, i.e. the antenna height was h.

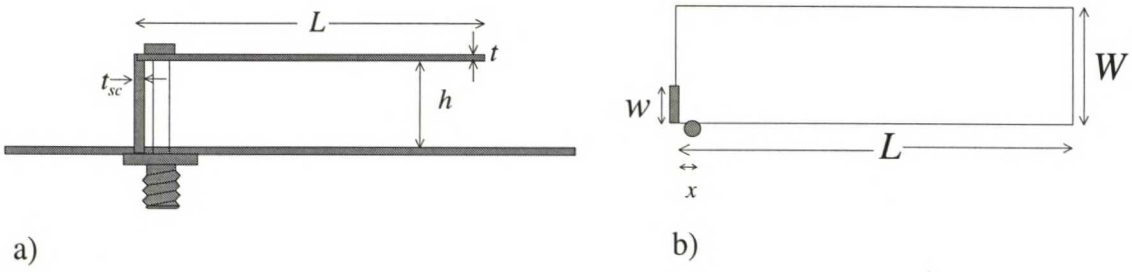

Figure 5.8 *Structure of the inductively loaded PIFA a) side view b) top view. L = 20 mm, t = t_{sc}= 0.5 mm, h = 5 mm, W = 10 mm, w = 1.5 mm, x = 1 mm.*

Capacitively loaded PIFA (PIFAC)

Structure of the capacitively loaded PIFA is shown in Figure 5.9. The radiating plate of size $L \times W$ and of thickness t was short-circuited to the ground plane by a copper wire of width w and thickness t. The short-circuit was located in the middle of the radiating plate edge. The open end of the radiating plate was folded toward the ground plane and a capacitive load plate of size $L_{CAP} \times W_{CAP}$ and of thickness t was soldered to it. The capacitive load was separated from the ground plane by a distance of d_{CAP}. The capacitively loaded PIFA was fed capacitively. The capacitive feed plate was a parallel plate of size $L_{CF} \times W_{CF}$ and it was separated from the radiating plate by a distance d_{CF}. The feed plate was connected into an SMA probe.

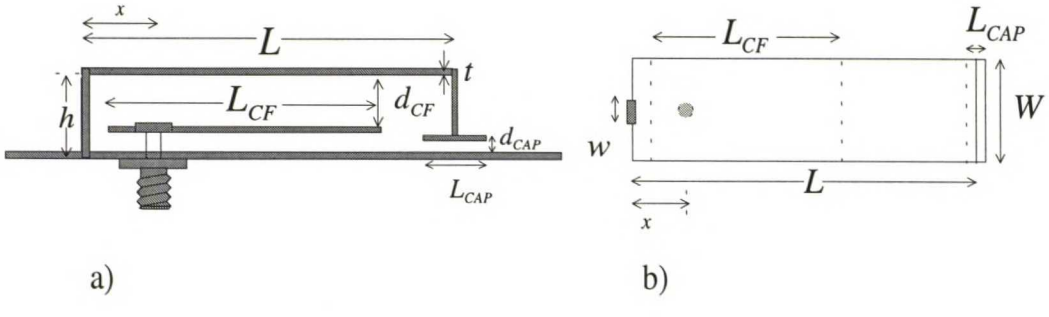

Figure 5.9 *Structure of the capacitively loaded PIFA a) side view b) top view. L = 20 mm, h = 5 mm, L_{CF} = 8 mm, d_{CF} = 2.5 mm, d_{CAP} = 2.5 mm, L_{CAP} = 2 mm, x = 5.6 mm, W = W_{CF} = W_{CAP} =10 mm, t= 0.5 mm.*

Meandered PIFAs (PIFAM1 and PIFAM2)

Two meandered PIFAs of the same kind were constructed. The structure is shown in Figure 5.10. The meandered radiating plate was implemented by cutting three narrow slits of width w_s and length s to a thin copper foil tape of size $L \times W$. The plate was set on a rigid foam plastic (Rohacell 51 HF, $\varepsilon_r' = 1.057$, $\tan\delta < 0.0002$) of height h. In the first prototype (PIFAM1) the SMA feed probe was at the corner of the radiating plate edge. In the second one (PIFAM2) the feed was at the distance of x_1 from the corner. In both prototypes, there was a short circuit strip of width w at a distance x_2 from the feed.

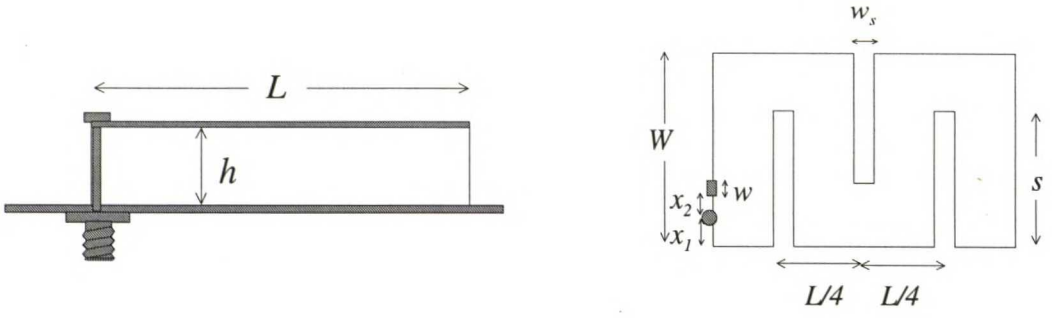

Figure 5.10 *Structure of the meandered PIFA a) side view b) top view. L = 20 mm, h = 5 mm, W = 10 mm, w= 1 mm, x_1= 0 mm (PIFAM1), x_1= 1 mm (PIFAM2), x_2= 1 mm, w_s = 1 mm, s = 8 mm.*

Resistively loaded PIFAs (PIFAR1 and PIFAR2)

The short circuits connecting the radiating plate and the ground plane in the meandered PIFA prototypes were replaced with chip resistors. In the first prototype (PIFAR1, i.e. PIFAM1 with the short circuit replaced with a chip-resistor), the DC value of the added chip-resistor was 4.7 Ω. At f = 2 GHz it was measured to have an equivalent circuit which in addition to the serial resistance included a serial inductance. The component values of this equivalent circuit were 7.2 Ω and 2 nH. The DC value of the chip resistor added in the second prototype (PIFAR2) was 2.2 Ω. At f = 2 GHz, the equivalent circuit of this resistor included components of 4.1 Ω and 1.6 nH.

Dielectrically loaded patch antenna (PAD)

The configuration of the dielectrically loaded patch antenna is shown in Figure 5.11. The radiating plate of size $L \times W$ was made of thin copper foil tape. It was fed by a probe located on the side of the radiating plate at distance x from the plate edge. The antenna was loaded with a slab of substrate material of $\varepsilon_{r1}' = 38$ and of size $L \times W$ with thickness h_1. The superstrate of size $L \times W$ and of thickness h_2 added on the radiating plate for gain enhancement was of $\varepsilon_{r2}' = 70$. The used dielectric materials were the same as the materials for constructing HV-DRAs.

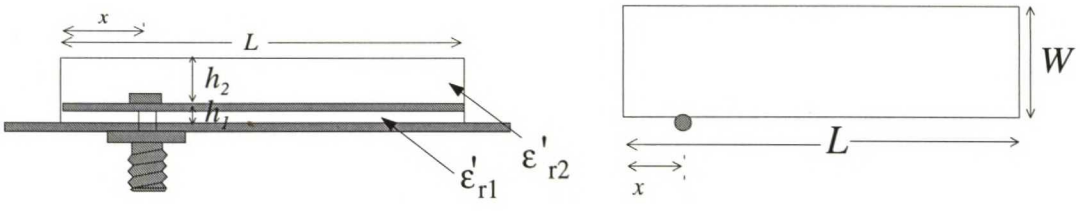

a) b)

Figure 5.11 *L = 20 mm, h_1 = 1.3 mm, h_2 = 3.8 mm, W = 10 mm, x = 5 mm, $\varepsilon_{r1}' = 38$, $\varepsilon_{r2}' = 70$.*

5.3.2 Reflection coefficients

The measured reflection coefficients as a function of frequency for the realized antennas are presented in Figure 5.12.

a) Inductively loaded PIFA

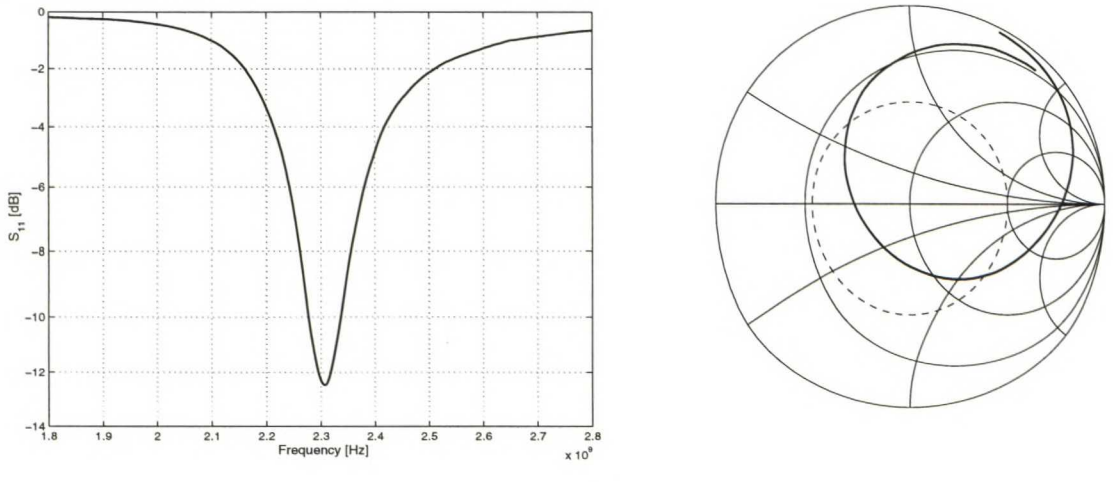

b) Capacitively loaded PIFA

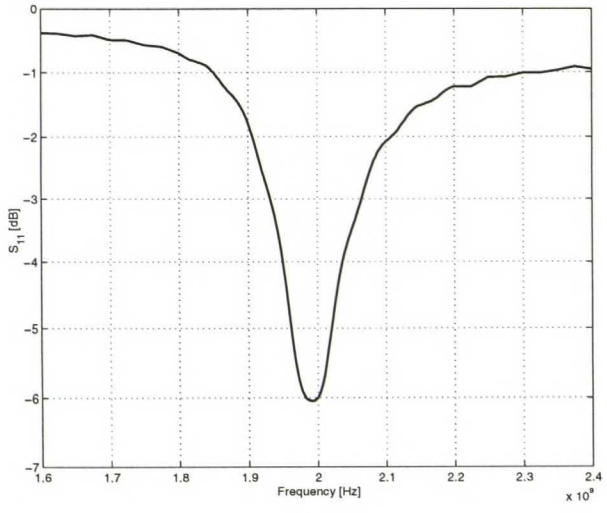

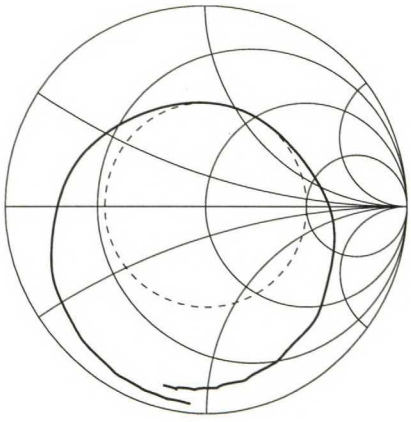

c) Meandered and resistively loaded PIFA 1

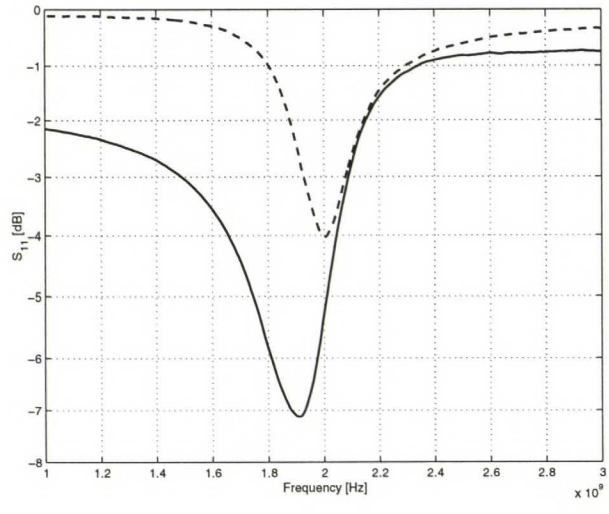

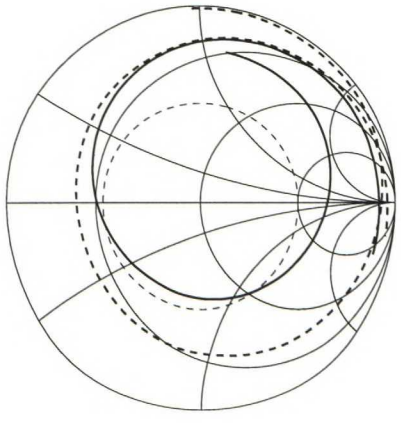

d) Meandered and resistively loaded PIFA 2

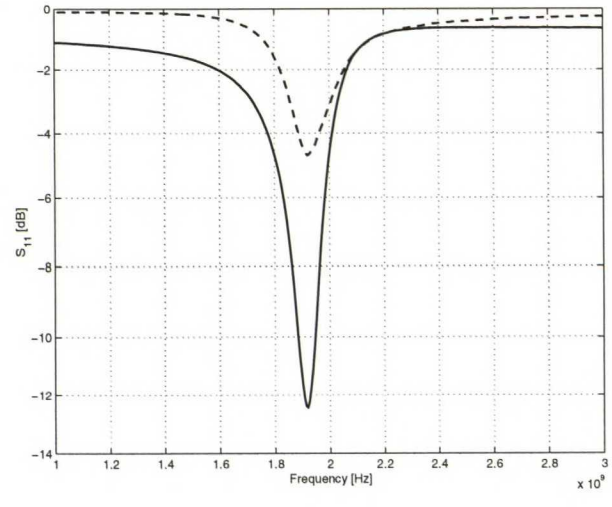

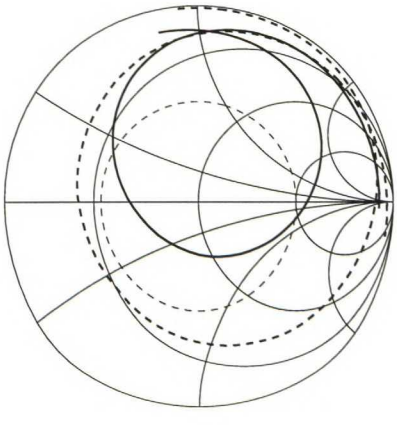

e) Dielectrically loaded patch antenna

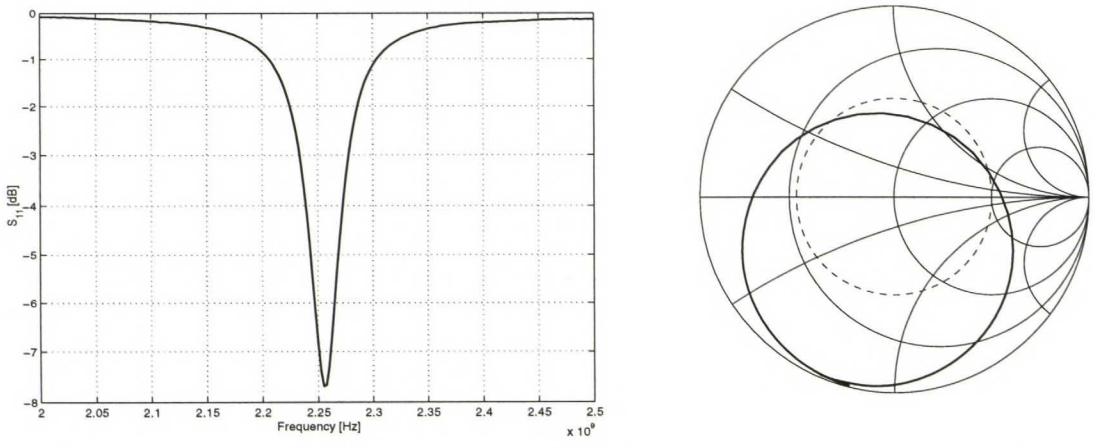

Figure 5.12 *Measured reflection coefficients for the a) inductively loaded PIFA, b) capacitively loaded PIFA, c) meandered and resistively loaded PIFA 1, d) meandered and resistively loaded PIFA 2, e) dielectrically loaded patch antenna. In Figures c and d, the dashed line represents the meandered PIFA and the solid line represents the meandered and resistively loaded PIFA. In Smith chart plots, the dashed line circle represents the reflection coefficient* $|\rho| = 0.501$ (L_{retn}= 6 dB).

Matching of the most prototypes was not near optimal as Figure 5.12 shows. Nevertheless, it was considered sufficient for further analysis and additional accommodation of the feed was not accomplished.

As can be seen from Figures 5.12c and 5.12d, the matching of the meandered PIFAs was markedly improved when a chip-resistor was added in the structure. Simultaneously the resonant frequency was slightly shifted because of the reactive part of the added chip resistor, and the shape of the reflection coefficient curve was changed due to the altered input impedance characteristics. It can also be observed that the bandwidth was clearly widened as a consequence of the added chip resistor.

The measured resonant frequencies for the prototypes are given in Table 5.7. The inductively and dielectrically loaded patch antennas had somehow higher resonant frequencies compared to others indicating that they had larger sizes in free space wavelengths than the other prototypes. Nevertheless, it should be remembered that the dielectrically loaded patch antenna was a $\lambda/2$-resonator while the others were $\lambda/4$-structures.

Table 5.7 *Measured resonant frequencies.*

Antenna	PIFA	PIFAC	PIFAM1	PIFAR1	PIFAM2	PIFAR2	PAD
f_r [MHz]	2308	1993	2006	1906	1919	1919	2255

5.3.3 Efficiency measurements

The measured radiation efficiency values for prototypes are presented in Table 5.8. The results obtained for PIFAs and the dielectrically loaded patch antenna with different caps agreed very well as was the case with DRAs. The uncertainty was ±1 percentage units.

Table 5.8 *Radiation efficiencies.*

Antenna	PIFA	PIFAC	PIFAM1	PIFAR1	PIFAM2	PIFAR2	PAD
η_r [%]	96±1	91±1	78±1	28±1	81±1	39±1	25±1

The inductively loaded PIFA had a very high radiation efficiency. The capacitively loaded PIFA had only slightly reduced efficiency compared to the inductively loaded one, as was expected (see Section 4.3.2). This reduction of efficiency was assumed to result from increased conductor losses and altered current distribution in the radiating plate due to the added load capacitor in the open end.

The two meandered PIFAs had somewhat equal radiation efficiencies. The efficiency decrease of theses structures compared to reactively loaded antennas is considered in the next subsection. Resistive loading was noted to decrease the efficiency greatly. The first meandered and resistively loaded PIFA prototype (PIFAR1) had a chip resistor with equivalent circuit of 7.2 Ω and 2 nH at 2 GHz. The second prototype (PIFAR2) had a chip resistor with equivalent circuit of 4.1 Ω and 1.6 nH at 2 GHz. It can be seen from the measured results that the radiation efficiency falls more for the larger resistance value, as is evident.

The dielectrically loaded patch antenna had a very low radiation efficiency. Further analysis for the reasons is presented in the next section. The same antenna structure was also measured without the superstrate layer on the radiating plate (see Figure 5.11). The resonant frequency was slightly shifted for this structure compared to the original dielectrically loaded patch antenna. The matching remained the same. In this case the

obtained efficiency value was η_r = (40±1)%. It was also found to be low even though it was higher than that of the original structure. In theory the superstrate is added on the radiating plate for radiation efficiency enhancement (see Section 4.2.3). Here, the size of the superstrate layer was probably improper, i.e. no resonance was excited inside the added structure, as no improvement but a reduction in the radiation efficiency was achieved.

5.3.4 Quality factor analysis

Experimental results for the quality factors are presented in Table 5.9. Q_0 for the resistively loaded PIFA (PIFAR1) was calculated by correcting the reflection coefficient curve symmetric (see Figure 5.12c). In this case the half power bandwidth B_{HP} = 214 MHz was estimated for the 2.77 dB - level.

The conductor quality factors were calculated using two different ways. Q_c was obtained as described in Section 5.1.3. Q_c' was calculated according to Equation (3.19) and using the effective conductivity value $\sigma_c = 3 \cdot 10^7$ S/m.

Table 5.9 *Experimental results for the quality factors.*

Antenna	PIFA	PIFAC	PIFAM1	PIFAR1	PIFAM2	PIFAR2	PAD
Q_0	21.8	40.8	32.0	6.7	35.6	14.9	139.6
Q_r	22.7	44.8	41.0	23.9	44.0	38.2	558.4
Q_d	-	-	5000	5000	5000	5000	3846
Q_c	550	457	150	9*	194	25*	196
Q_c'	2614	-	2437	2376	2384	2384	656
$Q_{c,ref}$	-	-	738	738	738	738	656
$Q_{d,glue}$	-	-	189	189	263	263	279

* Q_c includes the effects of the load resistors

There are significant differences in the values of Q_c and Q_c'. Several reasons can be found for the different values. In the calculation of Q_c' a uniform current distribution was assumed and the fields were assumed to be entirely between the radiating plate and the ground plane. In reality, the current distribution was not uniform and the fields were strongly expanded to the air. In addition, the calculation of Q_c' excluded the losses of the other metallic parts than the radiating plate and the ground plane, i.e. antenna feed and

the short circuit. Hence the values of Q_c are considered more reliable than the values of Q_c'.

The meandered, resistively and dielectrically loaded prototypes were constructed using copper tape for the radiating plate and for the short circuit. However, by constructing a reference meandered PIFA from copper plate of thickness t = 0.3 mm (PIFAM3), it was noticed that the glue of the tape introduced additional dielectric losses which needed to be considered. The reference antenna had the same dimensions than the tape-constructed meandered PIFAs but the slit length was s = 7 mm (instead of s = 8 mm) in this case. The short circuit was at the corner of the radiating edge, i.e. the structure was like PIFAM1 but the tape was replaced with copper plate (see Figure 5.10).

By this means it was found that meandering did not create losses but the losses in the meandered PIFAs resulted from the glue of the copper tape. The measured results for the reference copper plate PIFA are presented in Table 5.10.

Table 5.10 *Measured results for the copper plate meandered PIFA.*

Antenna	f_r *[MHz]*	η_r	Q_0	Q_r	Q_c
PIFAM3	2094	95±1	36.5	38.4	738

Actually the measured conductor quality factors of the meandered, resistively and dielectrically loaded antennas may be divided into contributions of the real conductor losses and the additional glue losses caused by the tape structure. The dielectric quality factors for the glue effects $Q_{d,glue}$ of the meandered and resistively loaded tape-PIFAs were calculated by taking the measured Q_c = 738 of the meandered copper plate PIFA as an assumption for the conductor quality factor value ($Q_{c,ref}$). Then the contribution of the glue losses could be excluded from the measured Q_c. Hence the glue quality factors $Q_{d,glue}$ = 189 and $Q_{d,glue}$ = 263 were obtained. For the dielectrically loaded patch antenna the theoretical conductor quality factor Q_c' = 656 was taken as an assumption for the conductor quality factor ($Q_{c,ref}$) as this structure does not contain a short circuit and the fields are more strongly between the radiating plate and the ground plane due to the dielectric loading and the low antenna profile. In this case, the glue quality factor $Q_{d,glue}$ = 279 was obtained.

When comparing the measured conductor quality factors of differently miniaturized prototypes, it can be noted that the conductor losses are larger in the capacitively loaded PIFA than in the inductively loaded one. This is due to increased metallic parts in the antenna structure and it is an expected result. The meandered PIFAs seem to have clearly larger measured conductor losses than reactively loaded PIFAs. The larger values are actually due to the glue of the tape. This explains also the decrease in the radiation efficiency of the meandered PIFAs compared to inductively and capacitively loaded ones. In the results for the resistively loaded PIFAs, the values of the conductor quality factors Q_c include the effects of the load resistors. For that reason the measured Q_c values are very low in these cases. The contribution of the measured conductor losses is found to be major in the case of dielectrically loaded patch antenna. Still, the absolute value of the conductor quality factor of the dielectrically loaded patch antenna was found similar to those of the meandered PIFAs for both cases with and without the glue losses.

As can be seen from the results in Table 5.9, the dielectric losses in all prototype structures were very small, in fact negligible (excluding the glue losses). In the case of dielectrically loaded patch antenna, the value of Q_d was calculated assuming that the fields were entirely between the radiating plate and the ground plane, i.e. in the $\varepsilon_{r1}' = 38$ material (see Figure 5.11).

5.3.5 Radiation patterns

The normalized radiation patterns for the prototypes are shown in Figure 5.13. The coordinate system is presented in Figure 5.2. The radiation patterns for the meandered PIFAs were not measured as the short circuits in these structures were replaced with chip-resistors before the pattern measurement was implemented. Nevertheless, the pattern shapes are assumed to be the same as for the resistively loaded PIFAs.

a) Inductively loaded PIFA, f = 2308 MHz

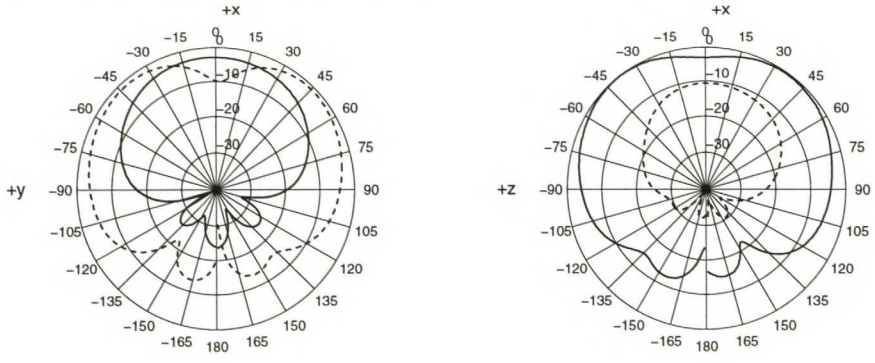

b) Capacitively loaded PIFA, f = 1993 MHz

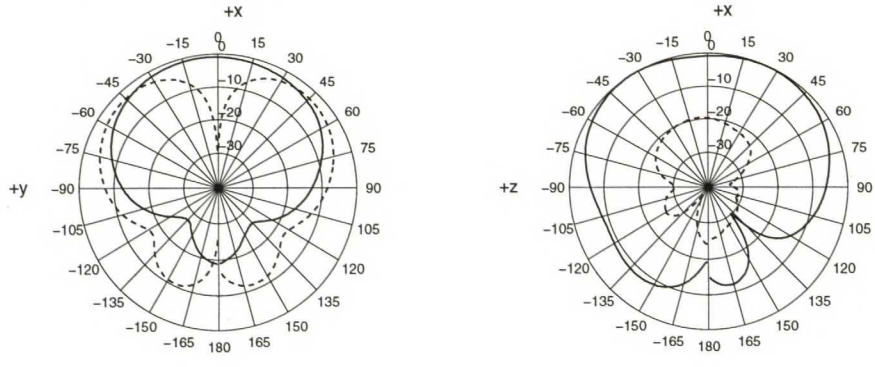

c) Resistively loaded PIFA 1, f = 1906 MHz

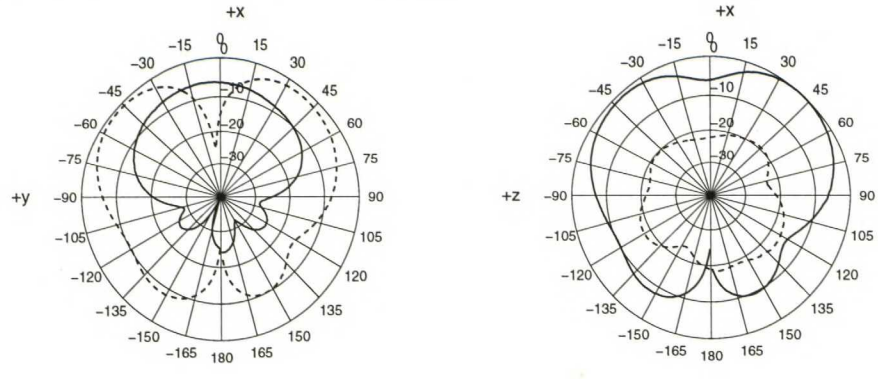

d) Resistively loaded PIFA 2, f = 1919 MHz

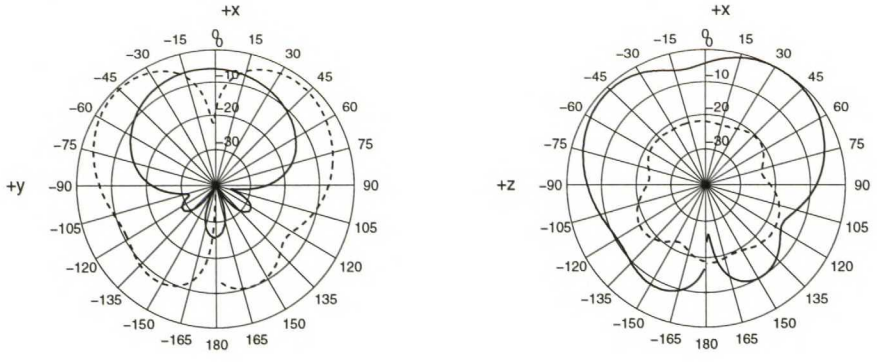

e) Dielectrically loaded antenna, f = 2255 MHz

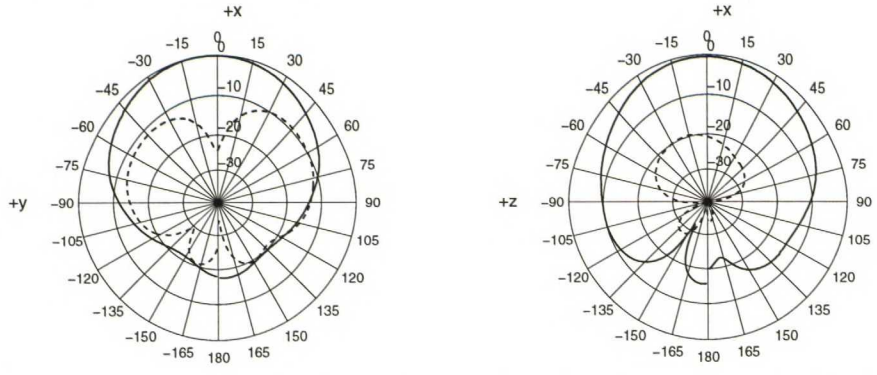

Figure 5.13 *Normalized radiation patterns for the a) inductively loaded PIFA, b) capacitively loaded PIFA, c) resistively loaded PIFA, 1 d) resistively loaded PIFA 2, e) dielectrically loaded patch antenna. Solid line represents the* E_θ*- component and dashed line the* E_ϕ*- component.*

It can be noticed from Figures 5.13a...5.13e that the radiation pattern shapes of differently miniaturized prototypes had some differences because of the changed current distribution in antenna structures. Still, as expected the radiation patterns of the two resistively loaded PIFAs resemble very much each other. Inductively and resistively loaded PIFAS had high cross-polarization level due to the direct radiation from the feed probe (see Figures 5.13a, c, d). In the capacitively loaded PIFA the cross-polarization level was lower resulting from the capacitive feed arrangement. That was the case also with the dielectrically loaded patch antenna as the feed probe length of this structure was only one fourth of the feed probe length in other prototypes. In addition, the radiation pattern of the dielectrically loaded antenna was found slightly more directive than the others.

5.3.6 Antenna gains

The measured antenna gains at resonant frequencies are given in Table 5.11. The limits for the uncertainty were approximated as described in Section 5.2.6.

Table 5.11 *Measured antenna gains.*

Antenna	**PIFA**	**PIFAC**	**PIFAM1**	**PIFAR1**	**PIFAM2**	**PIFAR2**	**PAD**
***G* [dB]**	5.2±1.1	5.1±1.1	-	0.0±1.1	-	1.5±1.1	0.6±1.1

The gain values for inductively and capacitively loaded PIFAs were regarded relatively large. The small difference in the values is supposed to be due to the difference in the radiation efficiency. The large gain values result partly from the large ground plane as was already discussed when dealing with HV-DRA gains in Section 5.2.6.

As the results in Table 5.11 show, the resistive load creates a significant gain reduction due to the decreased radiation efficiency. The larger the load resistor is, the smaller the antenna gain becomes as was the case also with radiation efficiency.

The dielectrically loaded patch antenna had a small gain, too. The gain is slightly larger compared to resistively loaded PIFA (PIFAR1) even though the radiation efficiency value of the dielectrically loaded patch antenna was lower. That is probably due to the more directive radiation pattern of the dielectrically loaded patch antenna.

For the dielectrically loaded structure without the superstrate on the radiating plate, a gain value of 2.1 dB was measured. The gain increase in this case is supposed to result from the higher radiation efficiency value.

5.4 SUMMARY OF THE MEASUREMENT RESULTS

Summaries of the main measurement results are presented in Tables 5.12 and 5.13.

Table 5.12 *Summary of the HV-DRA measurement results.*

ε_r'	**2.1**	**6.15**	**16**	**38**	**70**
f_r [MHz]	2075	2566	2172	2642	3005
η_r	99±1	95±1	93±1	89±1	86±1
Q_0	2.0	2.7	12.4	28.2	51.5
Q_r	2.0	2.8	13.3	31.7	59.9
Q_d	3333	526.3	1430	3890	1440
Q_c	213	88.3	129.3	273.3	492.9
G [dB]	7.8±1.1	6.2±1.1	5.6±1.1	5.8±1.1	5.2±1.1

Table 5.13 *Summary of the PIFA measurement results.*

Antenna	**PIFA**	**PIFAC**	**PIFAM1**	**PIFAR1**	**PIFAM2**	**PIFAR2**	**PAD**	**PIFAM3**
f_r [MHz]	2308	1993	2006	1906	1919	1919	2255	2094
η_r [%]	96±1	91±1	78±1	28±1	81±1	39±1	25±1	95±1
Q_0	21.8	40.8	32.0	6.7	35.6	14.9	139.6	36.5
Q_r	22.7	44.8	41.0	23.9	44.0	38.2	558.4	38.4
Q_d	-	-	5000	5000	5000	5000	3846	-
Q_c	550	457	150	9*	194	25*	196	738
$Q_{c,ref}$	-	-	738	738	738	738	656	-
$Q_{d,glue}$	-	-	189	189	263	263	279	-
G [dB]	5.2±1.1	5.1±1.1	-	0.0±1.1	-	1.5±1.1	0.6±1.1	-

* Q_c includes the effects of the load resistors

6 Discussion

In general the constructed prototypes showed that antenna size reduction results in a narrower bandwidth and a lower radiation efficiency. This was also found as a result of the literature study. In addition, the experimental work showed several detailed characteristics of the different miniaturization methods. In this chapter the obtained results of the work are discussed. First the essential issues relating to the miniaturization of dielectric resonator antennas are analyzed. Then the different miniaturization methods applied to planar inverted F antennas are discussed and compared. Finally, a conclusive summary is presented.

6.1 MINIATURIZATION OF DIELECTRIC RESONATOR ANTENNAS

Considering miniaturization, the effect of the material relative permittivity value on antenna performance is of interest as the wavelength in a material depends on the material permittivity value according approximately to $\lambda_r = \lambda_0/\sqrt{\varepsilon_r'}$ indicating that the greater the relative permittivity value is, the smaller the antenna size becomes (see Section 3.1.2). As a result of the literature survey, it was found that introduction of high permittivity material into an antenna structure worsens bandwidth characteristics and decreases radiation efficiency (see Section 4.2). To demonstrate this, a set of half-volume dielectric resonator antennas of different relative permittivity value but of the same geometrical shape were constructed. The material permittivity value varied from $\varepsilon_r' = 2.1$ to $\varepsilon_r' = 70$.

The measured results were not directly comparable due to variations in matching and resonant frequencies of the prototype antennas. To eliminate the effect of matching on bandwidth, unloaded quality factors were applied instead of bandwidth values as the relative bandwidth is inversely proportional to Q_0 and the quality of matching is included in the calculation of Q_0 [see Equation (2.17)]. However, either the unloaded quality factors were not directly comparable since the resonant frequencies of the prototypes differed noticeably. To be able to make an objective comparison considering antenna size and bandwidth, a frequency scaling had to be done. This was accomplished by presenting the antenna volume in wavelengths. As a result, bandwidth-to-volume-ratios $BW/V \propto Q_0^{-1} \cdot \lambda_0^3/V$ are shown in Table 6.1. Also the radiation efficiency values are shown in Table 6.1 in order to obtain a full coverage of the characteristics of different prototypes.

Table 6.1 *Bandwidth-to-volume-ratios and radiation efficiencies of the prototype DRAs.*

Antenna type	***BW/V***	η_r [%]
HV-DRA $\varepsilon_r' = 2.1$	30.8	99±1
HV-DRA $\varepsilon_r' = 6.15$	63.2	95±1
HV-DRA $\varepsilon_r' = 16$	95.5	93±1
HV-DRA $\varepsilon_r' = 38$	85.0	89±1
HV-DRA $\varepsilon_r' = 70$	79.6	86±1

To clarify the results in Table 6.1, the measured and theoretical radiation quality factor values for HV-DRAs with $\varepsilon_r' \geq 16$ were plotted in Figure 6.1. The prototypes of lower relative permittivity value were excluded due to their unclear resonant characteristics. In order to study purely the effect of the relative permittivity value on antenna performance (see Section 3.1.4), the measured Q_r values were normalized to the resonant frequency of the HV-DRA with $\varepsilon_r' = 16$, i.e. multiplied by $(f_r / f_{r,\varepsilon=16})^3$, hereby eliminating the variations in resonant frequencies of different structures [see Equation (3.12)]. The theoretical values were calculated assuming the measured Q_r value of the HV-DRA with $\varepsilon_r' = 16$ as a basis, and scaling the other Q_r values according to the theoretical dependency $Q_r \propto (\varepsilon_r')^{3/2}$ [see Equation (3.11)].

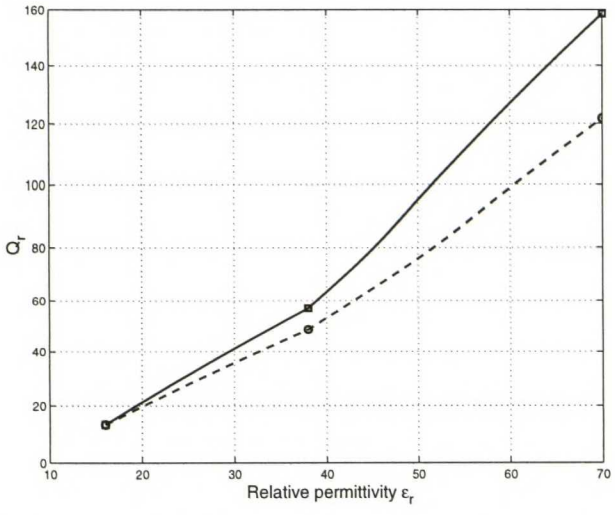

Figure 6.1 *Solid line with squares describes the measured values, dashed line with circles describes the theoretical values.*

It can be seen from Figure 6.1 that the measured radiation quality factors for antennas with $\varepsilon_r' \geq 16$ depend on relative permittivity value approximately according to theory, i.e. Q_r values are inversely proportional to antenna volume in wavelengths. As the theory applies for full-size DRAs, the slightly faster increase of the measured Q_r values is assumed to result from the half-volume structure or the inaccuracy in the theoretical model in general or both.

As can be found from the results in Table 6.1 and Figure 6.1, the behavior of the implemented antennas loaded with dielectric material was in accordance with the theoretical prediction. However, the bandwidth-to-volume ratio for HV-DRAs with ε_r' = 16...70 seems to decrease relatively slowly as a function of permittivity. The results show as well that the efficiency stays high also for high values of ε_r'. Hence there appears to be no limit in the miniaturization of DRAs indicating that if a drastic size reduction is required, DRAs could be a potential alternative.

The radiation pattern measurements showed that the radiation characteristics of the HV-DRA prototypes changed gradually from an electric dipole to a magnetic dipole when the relative permittivity value was increased from ε_r' = 2.1 to ε_r' = 70. This indicated that the prototypes with ε_r' = 2.1 and ε_r' = 6.15 did not have the actual characteristics of DRAs (see Section 4.2.2). Instead, in these two structures the direct radiation from the feed probe and/or the short circuit was assumed to dominate.

The measured HV-DRA gains decreased slightly with increased ε_r. That was mainly supposed to be due to the less directive pattern. The effect of a reduced η_r on gain was assumed to be small.

6.2 MINIATURIZATION OF PLANAR INVERTED F ANTENNAS

It was discovered from the literature study that the main difficulty in downsizing an antenna is the interrelation between antenna size, bandwidth, and radiation efficiency; an improvement in one property is always at the expense of some other (see Chapter 4). However, by applying different miniaturization methods, the trade-off contributions could be affected. In order to investigate the characteristics of different miniaturization techniques on antenna performance, a set of antennas each miniaturized applying a different method were tested. The selected antenna type was planar inverted F antenna as the common miniaturization methods were easily applicable for PIFAs, including inductive, capacitive, resistive, and dielectric loading, and a meandered radiating plate. The dielectrically loaded structure was actually not a PIFA but a $\lambda/2$-resonator. However, as the design criterion was to implement prototypes of the same physical size around the same resonant frequency, a short circuit could not be added to this antenna. Otherwise it would have had a resonant frequency approximately half of that of the other prototypes.

Since an objective comparison of differently miniaturized PIFAs was the purpose, the bandwidth-to-volume-ratios (obtained as described in Section 6.1) and radiation efficiency values for each prototype are presented in Table 6.2.

Table 6.2 *Bandwidth-to-volume-ratios and radiation efficiencies of the prototypes.*

Antenna type	***BW/V***	η_r [%]
PIFA (inductively loaded)	100.7	96±1
PIFAC (capacitively loaded)	83.6	91±1
PIFAM1 (meandered, tape-constructed)	104.5	78±1
PIFAM2 (meandered, tape-constructed)	107.3	81±1
PIFAM3 (meandered, copper plate-constructed)	80.6	95±1
PIFAR1 (resistively loaded)	582.0	28±1
PIFAR2 (resistively loaded)	256.4	39±1
PAD (dielectrically loaded patch)	16.9	25±1

It can be seen from the results in Table 6.2, that the inductively loaded PIFA has a very high radiation efficiency value and the bandwidth-to-volume-ratio seems relatively large. On the other hand, miniaturization to a much greater extent would probably not be possible using this method due to physical limitations in short circuit.

The results in Table 6.2 show as well that the capacitive loading of a PIFA lowers the efficiency slightly compared to inductively loaded PIFA. This effect was already found in the literature (see Section 4.3.2) and it is assumed to be due to increased metallic parts and changed current distribution resulting from the added capacitive load in the open end of the radiating plate. On the other hand, the capacitive load decreases the antenna size but this occurs at the expense of operating bandwidth. The achieved size reduction seems to be somewhat smaller than the wasted bandwidth. That would propose that much further miniaturization by capacitive loading would not be useful as the bandwidth became rapidly narrower.

The meandered, resistively, and dielectrically loaded prototypes were constructed using copper foil tape for the radiating plate and for the short circuit. However, by constructing a meandered PIFA of copper plate as a reference, it was noticed that the glue of the tape introduced additional dielectric losses, which needed to be considered. The estimated values of dielectric quality factors of the glue effects were calculated to be around $Q_{d,\,glue} \approx 200...300$ (see Section 5.3.4).

The meandered copper plate-PIFA was measured to have a very high radiation efficiency (see Table 6.2). By this means it was found that meandering itself did not create losses but the losses in the meandered tape-PIFAs resulted from the glue of the copper tape.

If the contribution of dielectric losses due to the tape glue was included in the results presented for the tape-constructed meandered PIFAs in Table 6.2, the properties of the antennas would change a bit; the bandwidth-to-volume-ratios would decrease and the radiation efficiencies would increase. Therefore, miniaturization by meandering the radiating plate of a PIFA seems to have a very high radiation efficiency. Still, the decrease in bandwidth worsens the overall performance of size reduction by this

technique. In addition, much further miniaturization (i.e. introducing more slits in the radiating plate) is assumed to be limited.

The results in Table 6.2 show that the performance of the reactively loaded and meandered PIFAs is more or less similar. By including the glue effects, the performance seems even more equal. It is worth noting that the total performance of the HV-DRA of $\varepsilon_r' = 16$ is also similar (see Table 6.1).

Introducing a chip resistor into an antenna instead of a short circuit is noted to clearly increase the operating bandwidth, as can be seen from the results in Table 6.2. However, this enhancement is directly at the expense of radiation efficiency, as is shown in the results and could also be found in the literature survey (see Section 4.4). It was found as well that the decrease in the radiation efficiency is proportional to the resistor value. By including the glue losses, the radiation efficiency would slightly increase and the bandwidth-to-volume-ratio would correspondingly decrease.

Even though dielectric loading seems to give good results with DRAs, it was not found useful with the patch structure realized in this work. Dielectrically loaded antenna has clearly worse bandwidth and radiation characteristics than the other prototypes even if the glue losses were also considered. Hence dielectric loading was observed not to be a suitable miniaturization method for a very low-profile structure with metallic parts, as the relative contribution of the metallic losses started to increase considerably when increasing high permittivity material into the structure due to very high radiation quality factor. Nevertheless, in the absolute sense the conductor losses were fairly similar in all constructed PIFA structures, including also the dielectrically loaded patch antenna. Thus, despite the exceptionally small bandwidth-to-volume-ratio as well as the radiation efficiency of the performed dielectrically loaded patch antenna, this may not be the case generally. The efficiency reduction reported in this work results partly from the added superstrate layer on the radiating plate as a dielectrically loaded patch antenna without the superstrate layer was as well tested and it had a radiation efficiency of $\eta_r = (40\pm1)$ %. The performance reduction may also be a consequence of a lower height of the basic structure than in the other prototypes. By filling a higher structure with dielectric

material this effect could be investigated. Such a structure will be considered in the future.

The implemented gain measurement showed that the gains were actually directly comparable to the radiation efficiencies, excluding the dielectrically loaded patch antenna, where the directivity was supposed to be slightly greater than in the other PIFA prototypes. The radiation efficiencies are plotted as a function of gain in Figure 6.2.

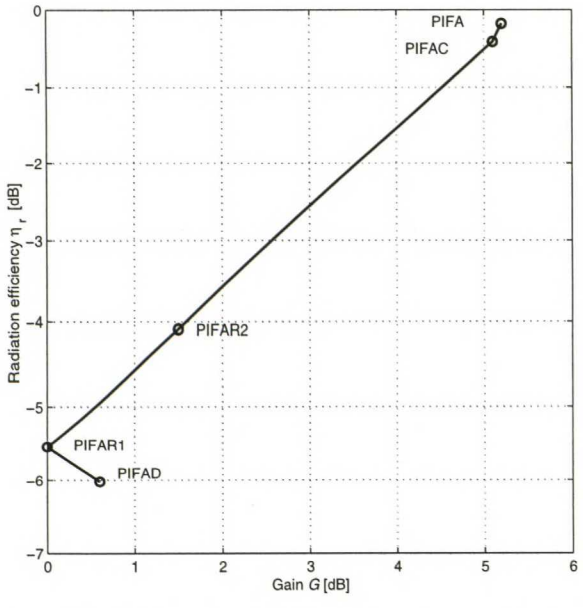

Figure 6.2 *Radiation efficiency as a function of antenna gain.*

6.3 CONCLUSIONS

The experimental work verified that the trade-off contributions of antenna size, bandwidth, and radiation efficiency could be affected by applying different miniaturization methods as the literature survey predicted. Nevertheless, none of the realized miniaturization techniques was observed to be more preferable than the others even though high permittivity DRAs seemed to be promising if a drastic size reduction was required. Similar set of DRAs has not been reported in the literature and thus this study offers novel and valuable knowledge. No theoretical or experimental comparison between miniaturization methods could either be found in the literature. Therefore the issues studied here give useful information about general miniaturization principles and the differences between the achieved antenna performance by applying different miniaturization methods.

7 Conclusions

Miniaturization techniques of handset antennas were studied in this master's thesis. The aim of the work was to investigate various miniaturization methods and to analyze the effects of different methods on antenna performance.

At first the general theory of small antennas was studied and requirements for handset antennas and theoretical limitations in size reduction were discussed. It was found that in general antenna size reduction results in a narrower bandwidth and a lower radiation efficiency. This was followed by an investigation of a few potential internal handset antenna types in the form of a literature survey. The study included the characteristics of dielectric resonator antennas and planar inverted F antennas. Relatively simple formulas concerning the miniaturization effects were found for DRAs but no such formulas could be found for PIFAs. Next the principles of different size reduction techniques were introduced and then the techniques were related to the studied antenna types.

The experimental work consisted of several prototype antennas. Prototypes included a set of half-volume dielectric resonator antennas of different permittivity value material ($\varepsilon_r' = 2.1...70$) but of the same geometrical shape, and a set of planar inverted F antennas each miniaturized applying a different method. In addition to the normal characterization of impedance and radiation properties, special emphasis was placed on the behavior of radiation efficiency.

According to the measurement results, the radiation quality factors of half-volume dielectric resonator antennas approximately followed the theoretical prediction of full-

sized structures. It was observed that the radiation quality factors were approximately inversely proportional to the volume of the resonator in wavelengths. The measurements showed as well that the efficiency stayed high for the high value of ε_r' also. This indicated that the bandwidth-to-volume-ratios decreased relatively slowly as a function of ε_r', which gives a good basis for the miniaturization of HV-DRAs.

The experimental results of different miniaturization methods applied to PIFAs showed that none of the techniques was clearly better than the others. However, it was noted that the trade-off contributions between antenna size, bandwidth, and radiation efficiency could be affected by applying different methods. The miniaturization of a very low-profile patch antenna by dielectric loading turned out to be useless as the radiation characteristics deteriorated and by that means the relative contribution of conductor losses grew considerably resulting in a very low efficiency. Resistive loading was observed to greatly increase the bandwidth but this occurred directly at the expense of radiation efficiency. The other implemented size reduction techniques were more or less equal in total performance. Miniaturization by reactive loading was discovered to have a high radiation efficiency but the achieved size reduction seemed to waste the bandwidth. The behavior of slow wave structures was found to be similar.

Since a basic research of the general behavior of differently miniaturized antennas was the purpose of this thesis, it can be stated that the goal was achieved well. In addition, this work has created several new ideas considering the development of small handset antennas. Further studies about low-profile DRAs should be done as the structures analyzed in this work do not have the desired shape for handset use. The results regarding the miniaturization of PIFAs suggest more detailed investigation in order to find an optimal solution. A thick dielectrically loaded PIFA as well as other dielectrically loaded structures containing metallic parts will be considered. Dielectric loading seems to be suitable for a drastic size reduction concerning DRAs but the performance of other techniques and antenna types should be tested as well. Future work is required also to study the special issues relating to multiresonant and multifrequency versions of miniaturized antennas. After solving the basic miniaturization problems, practical applications should be studied, e.g. the mechanics of the antenna and the effect of the user.

References

[1] E. Nyfors, P. Vainikainen, *Industrial Microwave Sensors*, Norwood, 1989, Artech House, 351 p.

[2] H. A. Wheeler, "The wide-band matching area for a small antenna", *IEEE Transactions on Antennas and Propagation*, Vol. 31, No. 2, March 1983, pp. 364-367.

[3] H. A. Wheeler, "Small antennas", *IEEE Transactions on Antennas and Propagation,* Vol. 23, No. 4, July 1975, pp. 462-469.

[4] K. Fujimoto, A. Henderson, K. Hirasawa, J. R. James, *Small Antennas*, New York, 1987, Research Studies Press, 305 p.

[5] H. A. Wheeler, "The radiansphere around a small antenna", *Proceedings of the IRE*, Vol. 47, No. 8, August 1959, pp. 1325-1331.

[6] J. D. Kraus, *Antennas*, 2nd ed., Singapore, 1988, McGraw-Hill, Inc., 892 p.

[7] J-P. Louhos, *Practical matching techniques for integrated antennas*, Seminar presentation, Helsinki University of Technology, Espoo, September 1998, 23 p.

[8] R. E. Collin, *Foundations for Microwave Engineering*, Tokyo, 1966, McGraw-Hill, Inc., 589 p.

[9] D. Kajfez, P. Guillon, (Eds.), *Dielectric Resonators*, Dedham, MA, 1986, Artech House, 539 p.

[10] H.F. Pues, A. R. van de Capelle, "An impedance-matching technique for increasing the bandwidth of microstrip antennas", *IEEE Transactions on Antennas and Propagation,* Vol. 37, No. 11, November 1989, pp. 1345-1354.

[11] C. A. Balanis, *Antenna Theory - Analysis and Design*, 2nd ed., New York, 1997, John Wiley & Sons, Inc., 941 p.

[12] R.C. Hansen, "Fundamental limitations in antennas", *Proceedings of the IEEE*, Vol. 69, No. 2, February 1981, pp. 170-182.

[13] R. E. Collin, S. Rothschild, "Evaluation of antenna Q", *IEEE Transactions on Antennas and Propagation,* Vol. 12, January 1964, pp. 23-27.

[14] J. McLean, "A re-examination of the fundamental limits on the radiation Q of electrically small antennas", *IEEE Transactions on Antennas and Propagation,* Vol. 44, No. 5, May 1996, pp. 672-676.

[15] R. E. Collin, "Minimum Q of small antennas", *Journal of Electromagnetic Waves and Applications*, Vol. 12, 1998, pp. 1369-1393.

[16] K. Fujimoto, J. R. James, *Mobile Antenna Systems Handbook*, Boston, 1994, Artech House, 617 p.

[17] A. Petosa, A. Ittipiboon, Y. M. M. Antar, D. Roscoe, M. Cuhaci, "Recent advances in dielectric-resonator antenna technology", *IEEE Antennas and Propagation magazine*, Vol. 40, No. 3, June 1998, pp. 35-48.

[18] Y. M. M. Antar, Z. Fan, "Theoretical investigation of aperture-coupled rectangular dielectric resonator antenna", *IEE Proc.-Microw. Antennas Propag.*, Vol. 143, No. 2, April 1996, pp. 113-118.

[19] R. K. Mongia, A. Ittipiboon, M. Cuhaci, "Measurement of radiation efficiency of dielectric resonator antennas", *IEEE Microwave and Guided Wave Letters*, Vol. 4, No. 3, March 1994, pp. 80-82.

[20] R. K. Mongia, A. Ittipiboon, "Theoretical and experimental investigations on rectangular dielectric resonator antennas", *IEEE Transactions on Antennas and Propagation*, Vol. 45, No. 9, September 1997, pp. 1348-1356.

[21] R. K. Mongia, A. Ittibipoon, M. Cuhaci, "Low profile dielectric resonator antennas using a very high permittivity material", *Electronics Letters*, Vol. 30, No.17, August 1994, pp. 1362-1363.

[22] R. K. Mongia, P. Bhartia, "Dielectric resonator antennas - A review and general design relations for resonant frequency and bandwidth", *International Journal of Microwave and Millimeter-Wave Computer-Aided Engineering*, Vol. 4, No. 3, 1994, pp. 230-247.

[23] S. A. Long, M. W. McAllister, L. C. Shen, "The resonant cylindrical dielectric cavity antenna", *IEEE Transactions on Antennas and Propagation,* Vol. 31, No. 3, May 1983, pp. 406-412.

[24] R. K. Mongia, "Theoretical and experimental resonant frequencies of rectangular dielectric resonators", *IEE Proceedings-H*, Vol. 139, No. 1, February 1992, pp. 98-104.

[25] M. W. McAllister, S. A. Long, G. L. Conway, "Rectangular dielectric resonator antenna", *Electronics Letters*, Vol. 19, No. 6, March 1983, pp. 218-219.

[26] R. A. Kranenburg, S. A. Long, "Microstrip transmission line excitation of dielectric resonator antennas", *Electronics Letters*, Vol. 24, No.18, September 1988, pp. 1156-1157.

[27] R. A. Kranenburg, S. A. Long, J. T. Williams, "Coplanar waveguide excitation of dielectric resonator antennas", *IEEE Transactions on Antennas and Propagation*, Vol. 39, No. 1, January 1991, pp. 119-122.

[28] K. Hirasawa, M. Haneishi, *Analysis, Design, and Measurement of Small and Low-Profile Antennas*, Boston, 1992, Artech House, 270 p.

[29] K.L. Virga, Y. Rahmat-Samii, "Low-profile enhanced-bandwidth PIFA antennas for wireless communications packaging, *IEEE Transactions on Microwave Theory and Techniques,* Vol. 45, No. 10, October 1997, pp. 1879-1888.

[30] J. R. James, P. S. Hall, C. Wood, *Microstrip Antenna Theory and Design*, London, 1981, Peter Peregrinus Ltd., 290 p.

[31] K. F. Lee, W. Chen (Eds.), *Advances in Microstrip and Printed Antennas*, New York, John Wiley & Sons, Inc., 1997, 599 p.

[32] G. A. E. Vandenbosch, A. R. Van de Capelle, "Study of the capacitively fed microstrip antenna element", *IEEE Transactions on Antennas and Propagation,* Vol. 42, No. 12, May 1994, pp. 1648-1652.

[33] I. Park, R. Mittra, "Aperture-coupled small microstrip antenna", *Electronics Letters*, Vol. 32, No. 19, September 1996, pp. 1741-1742.

[34] B. Belentepe, "Modeling and design of electromagnetically coupled microstrip-patch antennas and antenna arrays", *IEEE Antennas and Propagation Magazine*, Vol. 37, No. 1, February 1995, pp. 31-39.

[35] M. K. Tam, R. D. Murch, "Half volume dielectric resonator antenna designs", *Electronics Letters*, Vol. 33, No. 23, November 1997, pp. 1914-1916.

[36] T. K. Lo, Y. Hwang, "Bandwidth enhancement of PIFA loaded with very high permittivity material using FDTD", *IEEE AP-S International Symposium and URSI Radio Science Meeting*, Atlanta, Georgia, 1998, pp. 798-801.

[37] J. R. James, A. J. Schuler, R. F. Binham, "Reduction of antenna dimensions by dielectric loading", *Electronics Letters*, Vol. 10, No. 13, June 1974, pp. 263-265.

[38] S. Shum, K. Luk, "FDTD analysis of probe-fed cylindrical dielectric resonator antenna", *IEEE Transactions on Antennas and Propagation,* Vol. 46, No. 3, March 1998, pp. 325-333.

[39] R. K. Mongia, A. Ittipiboon, Y. M. M. Antar, P. Bhartia, M. Cuhaci, "A half-split cylindrical dielectric resonator antenna using slot-coupling", *IEEE Microwave and Guided Wave Letters*, Vol. 3, No. 2, February 1993, pp. 38-39.

[40] Y. Hwang, Y.P. Zhang, G.X. Zheng, T.K.C. Lo, "Planar inverted F antenna loaded with high permittivity material", *Electronics Letters*, Vol. 31, No. 20, September 1995, pp. 1710-1712.

[41] C.R. Rowell, R.D. Murch, "A capacitively loaded PIFA for compact mobile telephone handsets", *IEEE Transactions on Antennas and Propagation,* Vol. 45, No. 5, May 1997, pp. 837-842.

[42] C. R. R. Rowell, R. D. Murch, "A compact PIFA suitable for dual-frequency 900/1800 MHz operation", *IEEE Transactions on Antennas and Propagation,* Vol. 46, No. 4, April 1998, pp. 596-598.

[43] C. R. R. Rowell, R. D. Murch, "A capacitively loaded PIFA for compact PCS handsets", *IEEE AP-S International Symposium and URSI Radio Science Meeting*, 1996, pp. 742-745.

[44] K. Wong, K. Yang: Modified planar inverted F antenna, *Electronics Letters*, Vol. 34, No.1, January 1998, pp. 7-8.

[45] H. Chen, "Compact circular microstrip antenna with embedded chip resistor and capacitor", *IEEE AP-S International Symposium and URSI Radio Science Meeting*, Atlanta, Georgia, 1998, pp. 1356-1359.

[46] K. Wong, Y. Lin, "Small broadband rectangular microstrip antenna with chip-resistor loading", *Electronics Letters*, Vol. 33, No. 19, September 1997, pp. 1593-1594.

[47] P. Haapala, *Dual frequency helical antennas*, Master's thesis, Helsinki University of Technology, Espoo, Finland, June 1995, 62 p.

[48] F. Yang, X. Zhang, "Slitted small microstrip antenna", *IEEE AP-S International Symposium and URSI Radio Science Meeting*, Atlanta, Georgia, 1998, pp. 1236-1239.

[49] A. Lehto, A. Räisänen, *RF- ja mikroaaltotekniikka (RF and microwave engineering, in Finnish)*, Espoo, 1994, Otatieto, 250 p.

[50] Y. Yongzhao, J. Ollikainen, P. Vainikainen, "Simple but effective efficiency measurement method for small antennas", *URSI Remote Sensing Club of Finland / IEEE, XXIII National Convention on Radio Science and Remote Sensing Symposium*, 1998.

[51] G. S. Smith, "An analysis of the Wheeler method for measuring the radiation efficiency of antennas", *IEEE Transactions on Antennas and Propagation*, Vol. 25, No. 4, July 1977, pp. 552-556.

[52] G. P. Junker, A. A. Kishk, A. W. Glisson, D. Kajfez, "Effect of fabrication imperfections for ground-plane backed dielectric resonator antennas", *IEEE Antennas and Propagation Magazine*, Vol. 37, No. 1, February 1995, pp. 40-45.

[53] R. K. Mongia, A. Ittipiboon, M. Cuhaci, D. Roscoe, "Radiation Q-factor of rectangular dielectric resonator antennas: theory and experiment", *IEEE AP-S International Symposium and URSI Radio Science Meeting*, 1994, pp. 764-767.

[54] J. Ollikainen, *Multiresonant small planar antennas*, Master's thesis, Helsinki University of Technology, Espoo, Finland, March 1997, 128 p.